

EXPERIMENTAL TESTS OF BEAMS
WITH ECCENTRIC WEB OPENINGS

by

Jerry Lynn McNew

B. Arch., Kansas State University, 1973

A MASTER'S THESIS

submitted in partial fulfillment of the

requirements for the degree

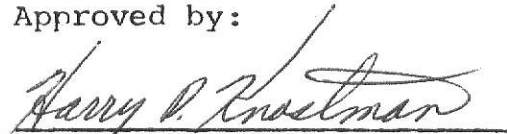
MASTER OF SCIENCE

Department of Civil Engineering

Kansas State University
Manhattan, Kansas

1974

Approved by:

A handwritten signature in dark ink, appearing to read "Harry D. Knutman", is written over a horizontal line.

Major Professor

**THIS BOOK
CONTAINS
NUMEROUS PAGES
WITH ILLEGIBLE
PAGE NUMBERS
THAT ARE CUT OFF,
MISSING OR OF POOR
QUALITY TEXT.**

**THIS IS AS RECEIVED
FROM THE
CUSTOMER.**

LD
2668
T4
1974
M33
C.2
Document

TABLE OF CONTENTS

	Page
List of Figures - - - - -	iii
List of Tables - - - - -	v
Nomenclature - - - - -	vi
Introduction - - - - -	1
Test Set-up and Test Procedure - - - - -	5
Introduction - - - - -	5
Specimen Description - - - - -	5
Instrumentation - - - - -	7
Test Set-up - - - - -	9
Test Procedure - - - - -	10
Theoretical Methods - - - - -	13
Numerical Integration Program - - - - -	13
Deflections - - - - -	16
Vierendeel Analysis - - - - -	18
Finite Element Analysis - - - - -	21
Elastic Test Results - - - - -	24
Deflections - - - - -	24
Strains - - - - -	25
Ultimate Load Test Results - - - - -	28
Introduction - - - - -	28
Beam 1 - - - - -	28
Beam 2 - - - - -	30
Conclusions - - - - -	33
Acknowledgements - - - - -	35
References - - - - -	36
Figures and Tables - - - - -	38
Abstract	

LIST OF FIGURES

	Page
Fig. 1 - Diagrams for Numerical Integration Program - - -	13, 15
Fig. 2 - Diagrams for Vierendeel Analysis - - - - -	19
Fig. 3 - Idealized Beam for Finite Element Method - - - -	22
Fig. 4 - Test Set-ups - - - - -	38
Fig. 5 - Opening and Reinforcement Details - - - - -	39
Fig. 6 - Tensile Specimen Details - - - - -	40
Fig. 7 - Cross-Section Dimension Locations - - - - -	41
Fig. 8 - Strain Gage Locations - Beam 1 - - - - -	45
Fig. 9 - Strain Gage Locations - Beam 2 - - - - -	46
Fig. 10 - Dial Gage Support Details - - - - -	47
Fig. 11 - Support Pedestal - - - - -	48
Fig. 12 - Load vs. Mid-span Deflection Elastic Load Tests - Beam 1 - - - - -	50
Fig. 13 - Load vs. Mid-span Deflection Elastic Load Tests - Beam 2 - - - - -	51
Fig. 14 - Stress Distribution Curves - Beam 1 - $M/V = 80$ -	52
Fig. 15 - Stress Distribution Curves - Beam 1 - $M/V = 60$ -	53
Fig. 16 - Stress Distribution Curves - Beam 1 - $M/V = 40$ -	54
Fig. 17 - Stress Distribution Curves - Beam 1 - $M/V = 20$ -	55
Fig. 18 - Stress Distribution Curves - Beam 2 - $M/V = 80$ -	56
Fig. 19 - Stress Distribution Curves - Beam 2 - $M/V = 60$ -	57
Fig. 20 - Stress Distribution Curves - Beam 2 - $M/V = 40$ -	58
Fig. 21 - Stress Distribution Curves - Beam 2 - $M/V = 20$ -	59
Fig. 22 - Load vs. Mid-span Deflection Ultimate Load Test - Beam 1 - - - - -	60
Fig. 23 - Load vs. Mid-span Deflection Ultimate Load Test - Beam 2 - - - - -	61

Fig. 24 - Mode of Failure - Beam 1 - - - - -	62
Fig. 25 - Interaction Curves - - - - -	63
Fig. 26 - Mode of Failure - Beam 2 - - - - -	64

LIST OF TABLES

	Page
Table 1 - Tensile Test Results - - - - -	40
Table 2 - Cross-Sectional Dimensions and Properties (At Opening) - - - - -	42
Table 3 - Cross-Sectional Dimensions (At Ends) - - - - -	44
Table 4 - Deflection Readings For 20 ^k Load - - - - -	49

NOMENCLATURE

Symbols

A	- cross-sectional area
E	- modulus of elasticity
F	- force
G	- shear modulus
I	- moment of inertia
L	- length
M	- moment
Q	- resultant force
P	- applied load
V	- shear
a	- half the distance between cross-sections
d	- length of moment arm
f	- stress
h	- depth
k	- kip
m	- moment due to unit load
t	- thickness
v	- shear due to unit load
x	- longitudinal distance from centerline of opening
y	- transverse distance from edge of i^{th} element to stress resultant
y	- transverse distance from centroidal axis to any fiber
z	- transverse distance from outer edge of flange to i^{th} element
δ	- deflection
σ	- normal stress

Subscripts

B - bottom section
N - net section
O - distance referring to moment-shear ratio
P - plastic
T - top section
b - bending
i - numerical designation
u - ultimate
w - web
1 - primary
1 - section including cover plates
2 - secondary

Abbreviations

HME - high moment edge
in. - inch, inches
ksi - kips per square inch
LME - low moment edge
N.A. - neutral axis

INTRODUCTION

As a result of the increasing trend toward economy in the construction of buildings, it is sometimes necessary to cut openings in the webs of structural steel members. These openings permit the passage of the mechanical and electrical systems of the building through supporting beams, thus reducing the space needed under the beams for duct work, pipes, and wiring, which reduces the required story height of the building. The need for most of these systems to remain essentially horizontal presents some problems when it becomes necessary to cut an opening in a structural member, as some of these openings will be concentric and others eccentric with respect to the longitudinal centerline of the beam.

Past investigations (1, 4, 5, 11) have been mainly concerned with reinforced and unreinforced concentric web openings, thus fairly well establishing methods which may be used to handle these cases. However, little attention has been given to the effect of eccentric openings on the strength of beams and no papers are known to have been published which deal with reinforced eccentric web openings.

To apply the Vierendeel method of analysis to beams with eccentric openings it is necessary to know the amount of the total shearing force that is carried by the sections of the beam above and below the opening. Equations to determine this distribution of shearing force are generally given as the nondimensional ratio V_T/V_B , where V_T and V_B are the shearing forces in the

top and bottom sections, respectively. Three recent papers have presented methods which may be used to determine this ratio.

Frost (10) conducted tests on four A36 steel W16 x 40 beams having unreinforced rectangular openings at different eccentricities and moment-shear ratios. Although considerable data was taken during these tests, he was unable to determine a consistent value for the shearing force distribution. Frost also developed an ultimate strength theory for beams with unreinforced eccentric web openings. This theory, which requires that the ratio V_T/V_B be known, predicts the maximum load carrying capacity of a beam. Frost's ultimate strength tests showed good agreement with this theory and supplied needed information on the failure mechanism at the opening.

Bower (2) uses data based on experimental tests conducted by Frost (8) to compare five different analytical methods for determining the shearing force carried by the top and bottom tee sections at unreinforced eccentric openings. Bower concluded that the best shear ratio was that determined by equating the shear deformations in the two sections when the shear coefficients of Cowper (6) are used. This conclusion is based on comparisons using data from Frost's (8) experiments, but the method used to determine these experimental results is not stated and Frost's reports (9, 10) do not contain these numerical values of the shear ratio.

Douglas and Gambrell (7) developed a design procedure for beams with unreinforced eccentric web openings based on inter-

action curves, which were derived using the Vierendeel method of elastic stress analysis and the von Mises yield theory. By treating the sections above and below the opening as fixed end beams connected to single beams at either end, they derived an equation for the shear ratio V_T/V_B . This equation is almost the same as that used by Frost (10), which was based on the relative stiffness of the two sections, except that Douglas and Gambrell used the shear coefficient of Cowper (6) to determine the shear deformation. Douglas and Gambrell conducted their tests on photoelastic models of beams with unreinforced eccentric openings. The comparison made of the Vierendeel stresses to those determined photoelastically is believed to be insufficient proof that this ratio of V_T/V_B is correct.

The present investigation deals with two beams having eccentrically positioned rectangular openings. The two beams were the same size and had the same size opening; the only difference between them was that the opening was reinforced in one case and unreinforced in the other. The two beams were each subjected to a series of elastic tests at four different moment-shear ratios, as well as an ultimate load test.

Both deflections and strains were recorded during the elastic tests. Deflections were measured at the middle of the beam and at the edges of the opening, for comparison with theoretical values. Longitudinal linear strains were measured at sections three inches either side of the vertical centerline of the opening. The cross-sectional stresses were determined from the strains and used in conjunction with

equilibrium equations to evaluate the shearing force carried by the sections above and below the opening.

The primary objective of the elastic tests was to determine, experimentally, the distribution of the shearing force to the sections above and below the opening, and the effect that the reinforcement had on this distribution. The ratio of the shearing force, V_T/V_B , was then compared to that predicted by the Finite Element Analysis and used to obtain stresses from the Vierendeel Analysis.

The ultimate load tests were conducted to observe the effects that the openings had on the behavior of the beams in the inelastic range and to compare the maximum load the beam could carry to that predicted by the ultimate strength theory. The ultimate strength method of solution results in interaction curves with the ratio of the moment at the opening centerline to the plastic moment of the gross beam (M/M_p) as the ordinate and the ratio of the shearing force at the opening to the plastic shearing force for the gross beam (V/V_p) as the abscissa. A moment-shear ratio (M/V) was used in these tests which intersected the interaction curves at a position which indicated the greatest variation between the curves for different areas of reinforcement. The moment-shear ratio (M/V) refers to the moment at the vertical centerline of the opening divided by the shearing force in the span, and is simply the distance from the support nearest the opening to the centerline of the opening.

TEST SET-UP & TEST PROCEDURE

Introduction

The experimental program was carried out on two W16 x 45 steel beams, 18 feet long, with a 6 inches deep by 9 inches long rectangular opening located at an eccentricity of 2 inches above the mid-depth of the beam. For all tests the beams were simple supported and a single concentrated load was applied at mid-span. Each beam was tested elastically at four moment-shear ratios, as shown in Fig. 4, and then an ultimate load test was conducted on each beam at a moment-shear ratio of 30 inches.

The opening in the first beam was unreinforced, while reinforcement was used on the second beam. The reinforcement consisted of steel bars located on one side of the beam, above and below the opening. Past investigations (4, 5) have indicated that one-sided reinforcement seems to be as effective in strengthening the beam as two-sided reinforcement.

Specimen Description

The beams were fabricated by a commercial steel fabricator. The openings were flame-cut using a machine template to a nominal size of 6 inches deep by 9 inches long, with a corner radius of $3/4$ inch. Vertical centerlines of the openings were located 24 inches from the centerline of the beams. The flame-cutting process yielded rough edges on the openings. Any irregularities, other than those caused by the flame-cutting, in the vicinity of the opening were noted before any tests were conducted.

Reinforcing bars for Beam 2 were made from 1/4 inch thick by 2 inch wide bar stock. This size of reinforcement was considered to be the practical minimum. It was considered not to be worthwhile to use bars less than this thickness and the width-thickness ratio of these bars is close to the upper limit for local buckling, according to the AISC Specifications (13). As indicated by the interaction curves in Fig. 25, this area of reinforcement causes sufficient variation, in the interaction curves, to be considered worth investigation. The bars were placed 1/4 inch from the top and bottom edges of the opening and were welded to the beam with 3/16 inch fillet welds. The welds ran the full length of the bars on the sides nearest the opening and were lapped back 1 1/2 inches at the ends. Extension of the bars beyond the edges of the opening was determined by the length of weld needed to develop the strength of the bars. All calculations of weld size and the strength of the bars were made in accordance to AISC Specifications (13). Reinforcement details are shown in Fig. 5.

In addition to the reinforcing, cover plates (4" x 24" x 5/16") were added to the top and bottom flanges of Beam 2 at the load point.

Tensile specimens (coupons) were taken from each beam and from the reinforcing bar stock. The coupons for the tensile tests were taken from a one foot lengths cut from one end of each beam, two from the web and two from each flange. As the reinforcing bars were both cut from the same length of bar stock, two one

foot lengths were cut from the same piece for the tensile tests. Figure 6 shows the locations from which the coupons were taken and their dimensions. Each tensile specimen was tested to determine its static yield point. Table 1 lists the results of these tests.

Before the beams were tested, the cross-sectional dimensions of the beams were measured at sections 3 inches to either side of the vertical centerline of the opening, as shown in Fig. 7. These dimensions were used in the numerical integration program and the Vierendeel Analysis, and are compared, along with the net cross-sectional properties, to the nominal dimensions and properties in Table 2. In addition, the cross-sectional dimensions were taken at the ends of the beams for use in the ultimate strength solution. These dimensions are shown in Table 3.

Instrumentation

During the elastic tests, data of two types were recorded, strains and deflections. Strains were obtained through the use of linear strain gages and deflections were measured with dial gages.

The strain gages used were 1/4 inch-gage length, epoxy-backed, foil-type, electrical resistant gages. All gages used were single linear type and were cemented to the beams parallel to the longitudinal axis of the beams, in the positions shown in Figs. 8 and 9. The centerline of the gages were 3 inches to either side of the vertical centerline of the opening. In all

forty gages were used on each beam. After the first series of tests on Beam 1, eight more gages were added to the top flange to determine the stress distribution across the flange. Strains were recorded using automatic and manual strain recording devices. Strains from thirty of the gages were recorded automatically and the other ten gages were recorded manually. The strains were recorded to determine the stress distribution through the sections above and below the opening.

Deflections were measured with mechanical dial gages with divisions of one-thousandth of an inch and a maximum deflection of 2 inches. The deflections were measured at the mid-span of the beams and at each edge of the openings with the gages positioned at the middle of the bottom flange. The gages were supported by a 4 inch steel channel, 18 feet in length. The channel and the beams were supported on the same pedestal, thus, eliminating the necessity for corrections to the deflection readings due to settlement of the support arms of the test machine. See Fig. 10 for details of the dial gage support system.

A coat of whitewash was applied to all surfaces of the beams. This coating has a property of cracking and flaking off with the mill scale when strains reach the yield level. Because of this property, the coating provided a qualitative method of visually following the sequence of yielding in the beam. It also facilitated in photographing the beams.

In the ultimate load tests, only the whitewash and the deflection gages were used, the whitewash to indicate regions

of yielding and the deflection readings, when plotted against load, to determine initial yielding and deflections at the ultimate load. When the beam deflections became large because of nonelastic action, the deflection readings were used to increment the loading of the beam.

Test Set-Up

Testing was conducted in a Tinius-Olsen screw type machine with a 200,000 pound loading capacity. Load was measured by a lever type load balancing arm. The pedestal supports for the beams were placed on the cantilever support arms of the machine.

The beams were simply supported on pedestals of the type shown in Fig. 11. They are rounded at the top to give, basically, a knife-edge support at the contact line between the beam and support. There is also a slight rounding of the base of the pedestal along the inside edge. These two conditions permit rotation of the beam about the support points as the load is applied. During the elastic tests the beams rested directly on the pedestal supports. However, during the ultimate load tests, bearing plates (6" x 7" x 1") were provided at the support points.

The load was applied at mid-span of the beam by a spherical loading head. A 3" x 7" x 1" bearing plate, with a 6" x 7" x 1/2" plate added later, was used under the load. There was no lateral support provided at any point along the beam, other than that provided by the friction created at the surfaces

between the bearing plates and the beams.

When a slight amount of web crippling was detected during the ultimate load test on Beam 1, testing was stopped and web stiffeners were provided at the load point before testing was continued. For the ultimate load test on Beam 2, web stiffeners were provided at the support points, as well as at the load point. These additional stiffeners were added because of the lateral buckling failure that occurred with Beam 1.

Test Procedure

In loading the test beams for the elastic tests, the loads were applied in varying increments, depending upon the moment-shear ratio span being tested. After each load increment was applied, readings of the strains and deflections were taken and recorded.

The load increment was determined by first calculating the maximum allowable elastic load, using the Vierendeel Analysis Method, and then dividing the maximum load into four equal loading increments. In the analysis for Beam 1, an allowable bending stress of 22 ksi and a shear distribution ratio (V_T/V_B) of 0.257, as determined from the equation given by Frost (10), were used. For Beam 1 these calculations gave maximum loads of 24, 28, 32, and 36 kips and load increments of 6, 7, 8, and 9 kips for the moment-shear ratios of 80, 60, 40, and 20, respectively.

In calculating the maximum loads for Beam 2, an allowable bending stress of 25 ksi was used, since tensile tests indicated the yield stress of the beams to be significantly greater than

36 ksi. Also, a shear distribution ratio of 0.4 was used, since the results of the tests on Beam 1 indicated that the ratio was greater than the 0.257 calculated above. The maximum loads for Beam 2, thus determined, were 35, 40, 48, and 50 kips for the moment-shear ratios of 80, 60, 40, and 20, respectively. A load increment of 10 kips was used in all tests on Beam 2, with only the maximum load varying in each case.

Before taking any data, the beams were loaded to a slightly higher value than the maximum load and then unloaded four or five times at each moment-shear ratio to eliminate the effects of residual stresses on the strain gage data. In the tests on Beam 1, all strain gages and deflection gages were "zeroed" with a load of 0 kips on the beam. However, by doing this the deflection and strain readings for the first load increment tended to be nonlinear with respect to the readings from the other load increments, thus the data from the first increment was neglected. This nonlinearity was due to the bottom flange of the beam being warped slightly, thus causing the beam to rock on the supports. Because of this nonlinearity, Beam 2 was loaded with an initial load before the gages were "zeroed".

The loading sequence went from the initial load to the maximum load and back to the initial load, with the loads being applied in increments. This method provided a check on the linearity of the gages and on the reproducibility of the data.

The ultimate load tests were conducted at a moment-shear ratio of 30 inches. This ratio was used because, as can be seen in Fig. 25, it is in the position of the "knee" of the interaction curve where the addition of reinforcement indicates the greatest theoretical effect on the ultimate load carrying capacity of the beam.

During the ultimate load tests, mid-span deflections were used to observe beam behavior. Applied loads were plotted against mid-span deflections, Figs. 22 and 23, to determine the onset of inelastic behavior. After inelastic behavior began, an applied load would drop off, with time, from a dynamic load to a static level. This static level was reached in 5 to 10 minutes. By loading with a screw-type machine, an imposed deflection would remain fixed after the crosshead was stopped, thus allowing a drop in load to be measured at a given deflection. These drops in load from the dynamic to the static level are indicated by the vertical lines in Figs. 22 and 23. In the inelastic range, loading varied according to an imposed deflection.

Loading was continued until the mode of failure was evident and the load began to decrease with an increase in deflection, thus indicating that the ultimate load carrying capacity of the beam had been reached.

THEORETICAL METHODS

Numerical Integration Program

In the vicinity of the opening the amount of shearing force distributed to the sections of the beam above and below the opening was determined through the use of a numerical integration computer program. This computer program converts the normal stresses at cross sections located equal distances either side of the opening centerline to the resultant shearing force acting on the section. The method was applied to the results of the experimental tests and the Finite Element solution. This distribution of the shearing force is required as input for the Vierendeel Solution.

To apply the numerical integration method it is necessary to determine the moment of the normal stresses at the section about the outside edge of the flange. Therefore, curves of the normal stresses are plotted, see Fig. 1a, and the area under the curve is divided into a number of smaller areas.

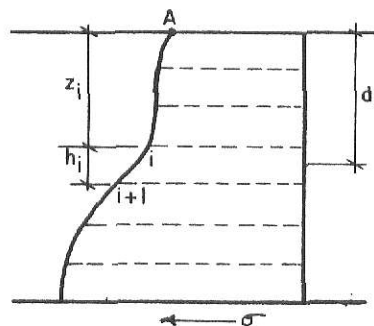


Fig. 1a

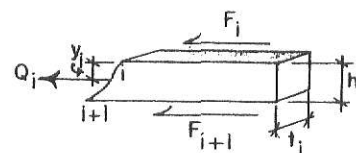


Fig. 1b

The depth of the area is designated h_i , which is not necessarily the same for each interval. The portion of the curve between points i and $i+1$ is assumed to be linear, thus forming a

trapezoidal area. Forces acting on the i^{th} trapezoidal element are F_i and F_{i+1} as shown in Fig. 1b, and are given by the stresses at points i and $i+1$ on the curve.

The resultant force, Q_i , acting on the element i is equal to

$$Q_i = \frac{(F_i + F_{i+1})(h_i)(t_i)}{2} \text{ ----- (1)}$$

in which t_i is the thickness of the element i . The total force, Q , acting on the section is the sum of all the element forces and is written as

$$Q = \sum Q_i \text{ ----- (2)}$$

The stress resultant Q_i acts through the centroid of the trapezoidal element which is indicated by the distance y_i in Fig. 1b and given by the equation

$$y_i = \frac{(F_i + 2F_{i+1})(h_i)}{3(F_i + F_{i+1})} \text{ ----- (3)}$$

If moments are taken about point A on the outer edge of the flange, the moment arm for the force Q_i is

$$d_i = z_i + y_i \text{ ----- (4)}$$

which is equal to the distance from point A to the centroid of the trapezoidal element. The distance z_i is simply

$$z_i = \sum h_{i-1} \text{ ----- (5)}$$

Then the moment of the force Q_i about point A is

$$M_i = (Q_i)(d_i) \text{ ----- (6)}$$

and the total moment created at the section about point A becomes

$$M = \Sigma M_i \text{ ----- (7)}$$

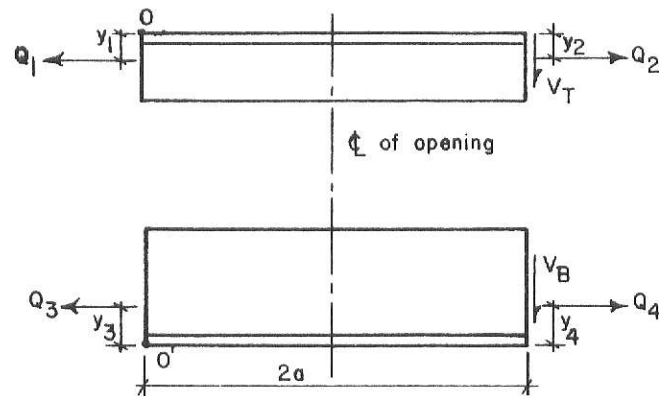


Fig. 1c

By establishing equilibrium of the top and bottom sections, in Fig. 1c, the values of V_T , the shear in the top section, and V_B , the shear in the bottom section, can be determined. Taking moments about point O gives the equation for the shearing force in the top section as

$$V_T = \frac{Q_2 y_2 - Q_1 y_1}{2a} \text{ ----- (8)}$$

where, a , equals half the distance between sections 1 and 2 and y_1 and y_2 locate the stress resultants on the sections. Since the moments, M , are equal to the Q 's times the y distances,

Eq. 8 can be written as

$$V_T = \frac{M_2 - M_1}{2a} \text{ ----- (8a)}$$

In the same manner, moments taken about point O' give the equation for the shearing force in the bottom section,

$$V_B = \frac{Q_3 y_3 - Q_4 y_4}{2a} \text{ ----- (9)}$$

or

$$V_B = \frac{M_3 - M_4}{2a} \text{ ----- (9a)}$$

The total shear, V, acting on the section is

$$V = V_T + V_B \text{ ----- (10)}$$

The results given by Eqs. 8 and 9 depend upon the load on the beam, but the proportion of the load carried by each section does not vary with the load within the elastic range. Hence, the distribution of shear to the top and bottom sections is generally expressed as the ratio V_T/V_B . It is this ratio that is required to apply the Vierendeel Method of Analysis and is used for comparison purposes between experimental and theoretical results.

Deflections

Mid-span deflections were predicted using the virtual work method. The effect of the opening and reinforcement were neglected in the calculations. In the calculations for the deflections of Beam 2, the effect of the mid-span flange cover

plates was taken into account.

By using the method of virtual work, the general equation for the mid-span deflection can be written as

$$\delta = \int_L \frac{Mm}{EI} dx + \int_L \frac{Vv}{A_w G} dx \text{ ----- (11)}$$

where δ is the deflection, M is the moment due to applied loading, m is the moment due to a unit load at mid-span, E is the modulus of elasticity (29,000 ksi), I is the moment of inertia of the gross beam section, V is the shear due to the applied loading, v is the shear due to a unit load at mid-span, A_w is the web area given by the beam depth times the web thickness, and G is the shear modulus (11,150 ksi).

Applying this equation to Beam 1, the mid-span deflection is given by

$$\delta = \frac{PL^3}{48EI} + \frac{PL}{4A_w G} \text{ ----- (12)}$$

where P is the applied load and L is the span length.

When Eq. 11 is applied to Beam 2, the equation for mid-span deflection becomes

$$\delta = \frac{P}{48E} \left[\frac{L^3}{I_1} + (L-L_1)^3 \left(\frac{1}{I} - \frac{1}{I_1} \right) \right] + \frac{P}{4G} \left[\frac{L}{A_{w1}} + (L-L_1) \left(\frac{1}{A_w} - \frac{1}{A_{w1}} \right) \right] \text{ ----- (13)}$$

where L_1 is the length of the cover plates, I_1 is the moment of inertia with the flange plates added, and A_{w1} is the web area found by taking the beam depth including the thickness of the cover plates times the web thickness.

Vierendeel Analysis

The Vierendeel Method of Analysis was first used in the analysis of trusses with vertical members perpendicular to the main longitudinal members of the truss. As it is applied to beams with web openings the following assumptions are made:

- 1) the beam sections above and below the opening are fixed at their ends (sections 1 and 2 in Fig. 2a),
- 2) points of inflection occur in the sections at the vertical centerline of the opening,
- 3) the amount of the shearing force to be distributed to the sections above and below the opening.

For concentric openings, the shearing force at the opening is assumed to be equally distributed between the upper and lower sections. However, for eccentric openings the total shearing force, V , must be proportioned between the unequal upper and lower sections and must satisfy the equilibrium requirement of Eq. 10. Formulas have been developed to assist in estimating values for this shearing force distribution, see Refs. (2) and (10).

By cutting the beam at the vertical centerline of the opening, where the points of inflection occur, the free-body diagram shown in Fig. 2b is obtained. Normal stresses at any distance x

**THIS BOOK
CONTAINS
NUMEROUS PAGES
WITH DIAGRAMS
THAT ARE CROOKED
COMPARED TO THE
REST OF THE
INFORMATION ON
THE PAGE.**

**THIS IS AS
RECEIVED FROM
CUSTOMER.**

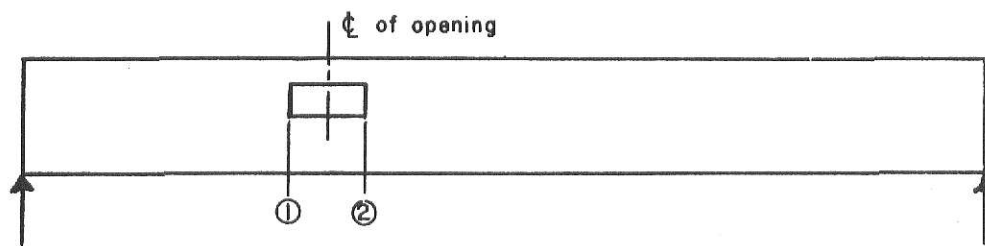


Fig. 2a

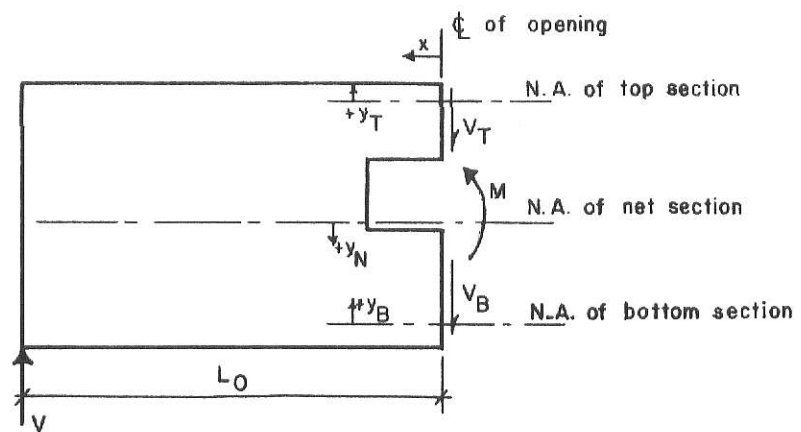


Fig. 2b

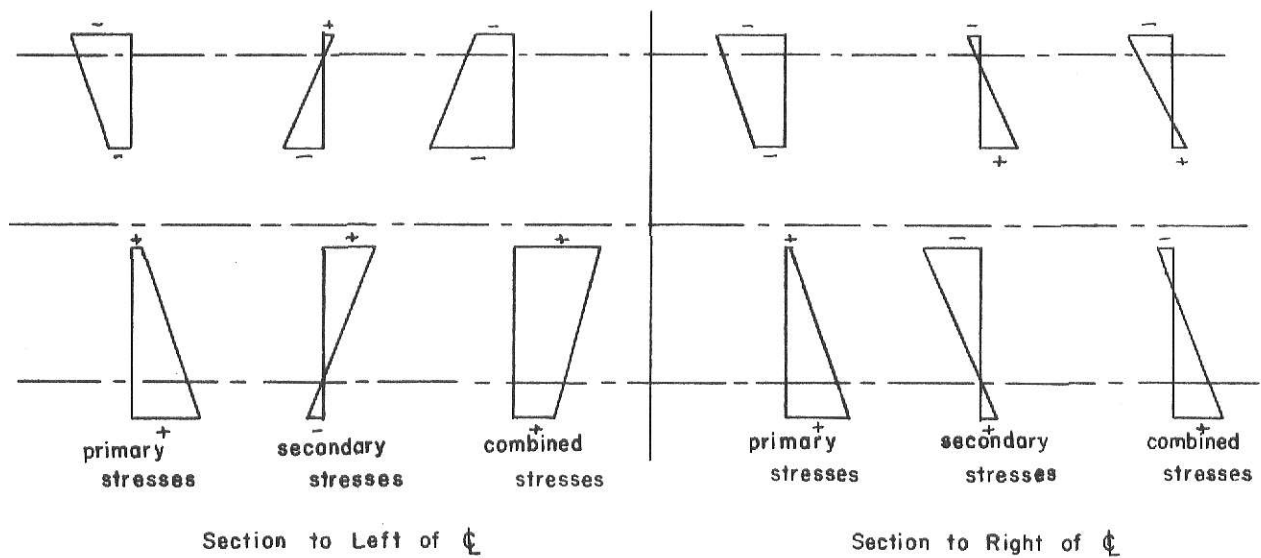


Fig. 2c

from the centerline are assumed to be composed of the stresses due to primary bending and Vierendeel (secondary) bending. The stress distribution caused by these moments is shown in Fig. 2c.

The primary bending moment creates a maximum compressive stress in the top fibers and a maximum tensile stress in the bottom fibers and is the same for all cross-sections at the opening. Stresses due to the primary bending moment, $M = V \cdot L_0$, are given by the flexure formula,

$$f_{b1} = \frac{My_N}{I_N} \text{-----} \quad (14)$$

where y_N is the distance from the neutral axis of the net beam section to any fiber, and I_N is the moment of inertia of the net section.

The secondary bending moments are caused by the shearing forces V_T and V_B times the distance from the point of inflection, x , to the cross-section. These secondary moments create stresses which are numerically equal at cross-sections equally spaced on either side of the centerline, but they are opposite in sign. The manner in which these stresses vary is shown in Fig. 2c. By substituting the expressions for the secondary moments into the flexure formula, the equation for the secondary bending stresses in the top section is found to be

$$f_{b2} = \frac{V_T(x)y_T}{I_T} \text{-----} \quad (15a)$$

or for the bottom section

$$f_{b2} = \frac{V_B(x)y_B}{I_B} \text{ ----- (15b)}$$

where y_T and y_B are the distances from the neutral axis of top or bottom section, respectively, to any fiber in the section, and I_T and I_B are the moments of inertia of the respective sections.

The general equation for the combined stress at any point in the top section is

$$f_b = \frac{My_N}{I_N} + \frac{V_T(x)y_T}{I_T} \text{ ----- (16a)}$$

and for the bottom section

$$f_b = \frac{My_N}{I_N} + \frac{V_B(x)y_B}{I_B} \text{ ----- (16b)}$$

Finite Element Analysis

The Finite Element method of analysis is one that is basically computer oriented. Although the method can be applied through hand calculations, it is best to use a computer because of the complexity of the matrices used in the method.

To apply the method, the beam is first idealized by dividing it into small areas, see Fig. 3, called elements. The smaller these elements, the better the accuracy that will be obtained. Each of these elements is connected to the others adjacent to it at points called nodes.

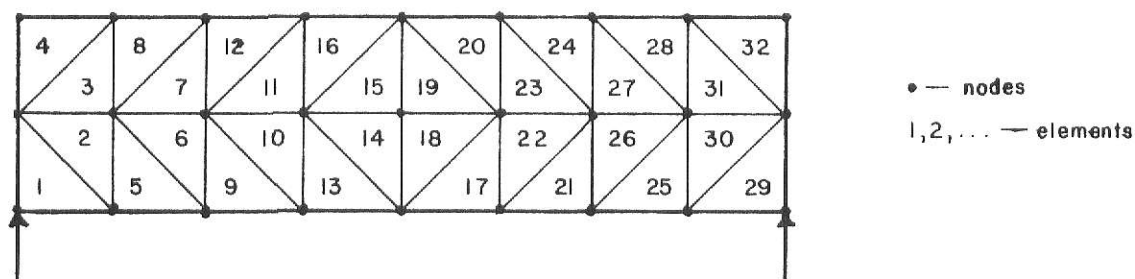


Fig. 3

For each of the elements the following assumptions are made in applying the method:

- 1) internal forces and displacements are related by material properties;
- 2) displacements at the boundaries of adjacent elements must be compatible; and
- 3) equilibrium must be satisfied for each element.

The idealization of the beam also includes concentrating the flange areas at approximately the extreme fibers and adjusting the areas such that the moment of inertia of the beam is unchanged. The area of any reinforcement is concentrated in a similar manner at its given centroidal location, with the area remaining unchanged as the moment of inertia is only slightly changed by such a concentration.

After the beam has been divided into these elements, the stiffness matrix for each of the elements is determined. These individual element stiffness matrices are then combined into the total stiffness matrix for the beam. By applying standard displacement method procedures, the displacements of

each node are determined. From these nodal displacements, the stresses in each of the elements are determined. The stresses thus determined are assumed to act at the centroid of their respective elements. Since the location of the centroids of all elements is known from the layout of the idealized beam, the stress distribution at any section can be plotted.

A detailed description of the exact method of the application of the Finite Element Method is given in Ref.(3).

ELASTIC TEST RESULTS

Deflections

Although deflections were not of primary interest in the elastic tests, deflection readings were recorded for each loading and unloading cycle. The readings were taken at the centerline of the beam and at each edge of the opening and recorded in Table 4. The results for the mid-span deflections are represented by the small circles shown in the load vs. deflection curves in Figs. 12 and 13. The values shown are the average of the deflections recorded for each load during each loading and unloading cycle. The deflections at each load all fall within the circle, when plotted individually. Since the steel channel supporting the dial gages, used to measure the deflections, was supported on the same pedestals as the beams no correction was necessary for support settlement. Theoretical deflections, shown by the solid lines in Figs. 12 and 13, were calculated using simple beam theory. In the calculations, the effects of the opening and any opening reinforcement was neglected, but the effects of shear deflection were taken into account. Nominal dimensions as shown in Table 2 were used in these calculations.

Referring to Figs. 12 and 13 it can be seen that the mid-span deflections predicted by theory very closely estimate the deflections at the higher moment-shear ratios and tend to underestimate the deflections at the lower moment-shear ratios. According to Vierendeel theory, this type of result can be

expected. The theory indicates that although the secondary deflections across the opening are the same for all moment-shear ratios, they become more important at the smaller moment-shear ratios, i.e., they represent a larger percentage of the total deflection. Thus the actual deflections could be more closely predicted by including the effects of the opening.

Strains

Normal strains were measured by strain gages located at two cross sections, 3 inches either side of the vertical centerline of the openings, as shown in Fig. 8 and 9. Normal stresses at these cross sections were determined by multiplying the measured linear strains by the modulus of elasticity (29,000 ksi).

Figures 14-21 show the curves representing the results of the experimental tests, the Finite Element Analysis solution and the Vierendeel Analysis for the beams for an applied load of 20 kips. More detailed descriptions of the Finite Element Analysis and the Vierendeel Analysis methods are given in the "Theoretical Methods" section. Stresses from the experimental tests are indicated by the small circles connected by solid lines. Each circle represents the average stress of the two gages which lie opposite each other on the web and the flanges. If the individual stress from each gage is plotted at its location it will fall within the circle at that point. The stresses predicted by the Finite Element Analysis are indicated

by the broken lines, and those predicted by the Vierendeel Analysis are shown by the dashed lines. As indicated in the explanation of the Vierendeel Analysis it is necessary to know the shear distribution to the top and bottom sections. The shear distribution used for these Vierendeel analyses was that determined from the experimental results, using the numerical integration program.

The curves show that agreement between the experimental results and those predicted by the two theories is quite good in all cases except in the top section at the high moment edge for which the agreement is not as good. However, this disagreement is acceptable if one looks mainly at the agreement between the three curves in the vicinity of the highest stresses for each section, in which case the theoretical methods predict the stresses fairly accurately. It may also be noted that the Finite Element Analysis tends to overestimate the stress concentrations at the top and bottom edges of the openings. The Vierendeel Analysis tends to underestimate the stresses at the top and bottom edges of the openings since it does not take into account the effects of any stress concentrations.

The normal stresses from the elastic tests and the Finite Element Analysis curves were numerically integrated to determine the shearing force present in the sections above and below the opening. These values were then used to determine the ratio of the shearing force carried by the upper section to that of the lower section. The integration process indicated

a total shear force across the opening of 8.58 kips and 9.42 kips for Beams 1 and 2, respectively. Although these forces are not equal to the 10 kips present because of the loading test set-up, equilibrium checks conducted on both beams using the resultant forces, from the integration, indicated beam equilibrium within 5 percent. The shear distribution ratio was found to be essentially independent of the moment-shear ratio. The results of the integration gave average shear distribution ratios of 0.375 (experimental) and 0.360 (finite element) for Beam 1 and 0.328 (experimental) and 0.380 (finite element) for Beam 2. The average actual dimensions, shown in Table 2, were used in the numerical integration program to determine the experimental shear distribution ratios. Nominal dimensions, with the flange areas adjusted to account for the position of the flanges, were used in the Finite Element solution.

By integrating the shear stresses produced in the Finite Element Analysis, the shear distribution ratios are 0.373 and 0.391 for Beams 1 and 2, respectively.

ULTIMATE LOAD TEST RESULTS

Introduction

As previously described, both beams were whitewashed with the mill scale intact. This provided a visual means of observing yielding as it progressed through the beams. In addition, the deflection gages were used to provide the data for the load vs. mid-span deflection curves shown in Figs. 22 and 23. These curves give the loading histories of the beams. In these figures, the small circles indicate the static load levels, the tops of the vertical lines above the circles indicate the dynamic load levels and the dashed lines show the corrections for strain hardening.

Both beams were tested at a span of 108 inches, corresponding to a moment-shear ratio of 30 inches. Web stiffeners were placed at the load points of both beams after slight web crippling occurred at that point during the first attempt to load Beam 1 to failure, but before any significant yielding had occurred elsewhere in the beam. On Beam 2, stiffeners were placed at the support points also.

Beam 1

The loading history for Beam 1, after the web stiffeners were added at the load point, can be followed from the load vs. mid-span deflection curves in Fig. 22.

Yielding was first indicated by the flaking of whitewash in the vicinity of the corners of the opening at the high moment edge at a static load of 128.2 kips (load No. 6). Yield-

ing became more advanced in this region at load No. 7 (136.7^k). At load No. 9 (150.0^k), yielding had begun in the upper corner of the opening at the low moment edge and in the compression flange in the area of the opening. By the time the maximum dynamic load (156.9^k) was reached at load No. 10 the beam had begun to buckle laterally in such a way that the compression flange remained essentially straight while the ends displaced sideways and the tension flange remained in contact with the supports and didn't appear to be displaced laterally. After this the lateral buckling progressed rapidly with a decreasing load, therefore failure was attributed to lateral buckling at a maximum static load of 150.3 kips (load No. 10). Figure 24 illustrates the mode of failure attained and the yield patterns obtained by the time of failure.

The interaction curve, based upon ultimate strength theory (12), which predicts the ultimate load for Beam 1 is shown in Fig. 25. The predicted ultimate strength of a beam is dependent upon the shearing force and the bending moment at the centerline of the opening. By plotting a line representing the moment-shear ratio from the origin of the interaction curve, the ultimate load for the beam is determined by its intersection with the curve. The small solid circle in the figure indicates the experimental ultimate load, which corresponds to the moment and shear ratios used as the interaction curve coordinates. According to the interaction curve the predicted ultimate load for Beam 1 is 128.9 kips, whereas the experimental load at failure was 150.3 kips. This result indicates that the ultimate

strength theory underestimated the failure load by 16.6 percent. This percentage of difference is slightly misleading in that the ultimate strength theory used to develop the interaction curve neglects the effect of strain hardening on the load carrying capacity of the beam.

By drawing two lines tangent to the flat portions of the load vs. mid-span deflection curve (Fig. 22), the load at which strain hardening began can be approximated. This is a rough approximation for Beam 1 in that the premature failure by lateral buckling did not permit determination of the actual upper flat portion of the curve with much accuracy. With this correction, the ultimate load for Beam 1 indicated by the small open circle, neglecting strain hardening, is determined to be 135.2 kips. Comparing this load to the 128.9 kips, predicted by theory, gives an underestimate of 4.9 percent on the ultimate load for the beam.

Beam 2

For the ultimate load test of Beam 2, web stiffeners were added at the support points, in addition, to the stiffeners at the load point. The stiffeners at the support points were added in an attempt to confine the failure to the vicinity of the opening and prevent lateral buckling. The load history for Beam 2 is shown in Fig. 23.

Initial yielding occurred at the static load of 118.2 kips (load No. 5) at the bottom corner of the opening at the high moment edge. By load No. 8 (146.6^k), yielding had developed in the web area between the reinforcing bars, as indicated by

lines of whitewash flaking progressing from the edge of the opening outward. At a load of 153.8 kips (load No. 9) yielding had begun in the reinforcing bar above the opening at the high moment edge. Yielding continued to progress fairly rapidly in the areas already indicated, also moving into the reinforcement at the other corners of the opening, until at load No. 15 (182.6^k) when the compression flange at the high moment edge of the opening began to buckle laterally. The maximum dynamic load (191.2^k) was reached while changing from load No. 16 to load No. 17, as the load began to drop off during loading. The static load causing failure was taken as 184.6 kips (load No. 16) and the mode of failure was attributed to lateral buckling of the compression flange in the vicinity of the high moment edge of the opening. Figure 26 shows the mode of failure and yield patterns for Beam 2.

From the interaction curve for Beam 2, shown in Fig. 25, the predicted ultimate load was 152.2 kips. This predicted load is 21.4 percent less than the experimental failure load of 184.8 kips, indicated by the small solid square. As with Beam 1, this percentage is misleading. Correction for strain hardening gives an experimental ultimate load of 154.6 kips, indicated by the small open square. This is an underestimate of 1.6 percent of the ultimate load carrying capacity of the beam.

Although both beams failed by a form of lateral buckling, it is felt that the presence of the web stiffeners at the supports points helped to confine the lateral buckling to the

compression flange in the vicinity of the opening, for Beam 2, instead of spreading throughout the length of the beam, as happened with Beam 1.

CONCLUSION

From the experimental tests conducted in this investigation the following conclusions can be made:

1. Mid-span deflections can be reasonably estimated using simple beam theory and including the effects of shear but neglecting the effects of the opening and any reinforcement.
2. Normal stresses predicted using the Finite Element or Vierendeel Methods of Analysis are, in most cases, in good agreement with those obtained experimentally. It is therefore felt that either of these methods of analysis can reasonably be used in the design of beams with eccentrically positioned unreinforced and reinforced web openings.
3. The moment-shear ratio has very little effect on the ratio of the shearing force carried by the beam section above the opening to that carried by the section below the opening. It also had little effect on the general shape of the stress distribution curves for the same load. However, this ratio did cause the curves to be displaced and rotated slightly with respect to each other.
4. The presence of reinforcement at the opening tends to reduce the magnitude of the stresses at the opening edges.

5. Irregularities along the opening edges, caused by the flame-cutting of the opening, had no noticeable effect on the elastic behavior and ultimate strength of the beam.
6. The difference between the experimental and theoretical failure loads can be partly attributed to the effects of strain hardening, as the ultimate strength theory used does not include the effects of strain hardening.
7. The load carrying capacity of the beam can be fairly accurately predicted using the ultimate strength theory presented in Ref. (12). This theory is the most recent known to be available.
8. Addition of reinforcement in the vicinity of the opening significantly increases the maximum load carrying capacity of the beam.*
9. Agreement between the shear distribution ratios, V_T/V_B , obtained from the Experimental results and the Finite Element Analysis was not too consistent. It is recommended that this agreement be further investigated in future experiments.

*The predicted loads indicated an increase of 18 percent with the addition of reinforcement, whereas the results of the experimental tests showed an increase of 23 percent.

ACKNOWLEDGEMENTS

Support for the research described in this report was provided by National Science Foundation Grant GK-35762 and the Department of Civil Engineering at Kansas State University. This support is gratefully acknowledged.

The author wishes to express sincere appreciation to Dr. Harry D. Knostman for serving as major advisor and for assistance in conducting the experimental tests and in the preparation of this report.

Appreciation is also extended to Dr. Peter B. Cooper for providing the ultimate strength theory information used in this report and for serving on the advisory committee.

Appreciation is extended to Dr. Robert R. Snell, Head of the Department of Civil Engineering, and Dr. Stuart E. Swartz for serving as members of the advisory committee.

Thanks is also given to Mr. Eric Schoeff for assistance in the preparation of the beams for testing.

REFERENCES

1. Bower, J. E., "Ultimate Strength of Beams with Rectangular Holes," Journal of the Structural Division, ASCE, Vol. 94, No. ST6, Proc. Paper 5982, June, 1968, pp. 1315-1337.
2. Bower, J. E., "Analysis and Experimental Verification of Steel Beams with Unreinforced Web Openings," University of Wisconsin Institute on "Design of Beams with Web Openings," January 22-23, 1970.
3. Brice-Nash, R. L., Snell, R. R., and Cooper, P. B., "Shear Force Distribution in Beams with Eccentric Web Openings by the Finite Element Method," Research Project Report, Dept. of Civil Engineering, Kansas State University, May, 1974.
4. Congdon, J. G., and Redwood, R. G., "Plastic Behavior of Beams with Reinforced Holes," Journal of the Structural Division, ASCE, Vol. 96, No. ST9, Proc. Paper 7561, September, 1970, pp. 1933-1956.
5. Cooper, P. B., and Snell, R. R., "Tests of Beams with Reinforced Web Openings," Journal of the Structural Division, ASCE, Vol. 98, No. ST3, Proc. Paper 8791, March, 1972, pp. 611-632.
6. Cowper, G. R., "The Shear Coefficients in Timoshenko's Beam Theory," ASME Transactions, Series E, Vol. 33, June, 1966, Journal of Applied Mechanics, pp. 335-340.
7. Douglas, T. R., and Gambrell, S. C., Jr., "Design of Beams with Off-Center Web Openings," Journal of the Structural Division, ASCE, Vol. 100, No. ST6, Proc. Paper 10611, June, 1974, pp. 1189-1203.
8. Frost, R. W., Unpublished Data, U.S. Steel Applied Research Laboratory, Monroeville, PA., 1969.
9. Frost, R. W., "The Behavior of Steel Beams with Eccentric Web Holes," presented at ASCE Structural Engineering Conference, St. Louis, MO, October 21, 1971.
10. Frost, R. W., "Behavior of Steel Beams with Eccentric Web Holes," Technical Report 46.019-400 (1), Research Laboratory, United States Steel Corporation, February, 1973.
11. Redwood, R. G., and McCutcheon, J. O., "Beam Tests with Unreinforced Web Openings," Journal of the Structural Division, ASCE, Vol. 94, No. ST1, Proc. Paper 5706, January, 1968, pp. 1-17.

12. Wang, Tsong-Miin, Snell, R. R., and Cooper, P. B.,
"Strength of Beams with Eccentric Reinforced Holes,"
Research Project Report, Dept. of Civil Engineering,
Kansas State University, July, 1974.
13. "Manual of Steel Construction," American Institute of
Steel Construction, New York, 1970.

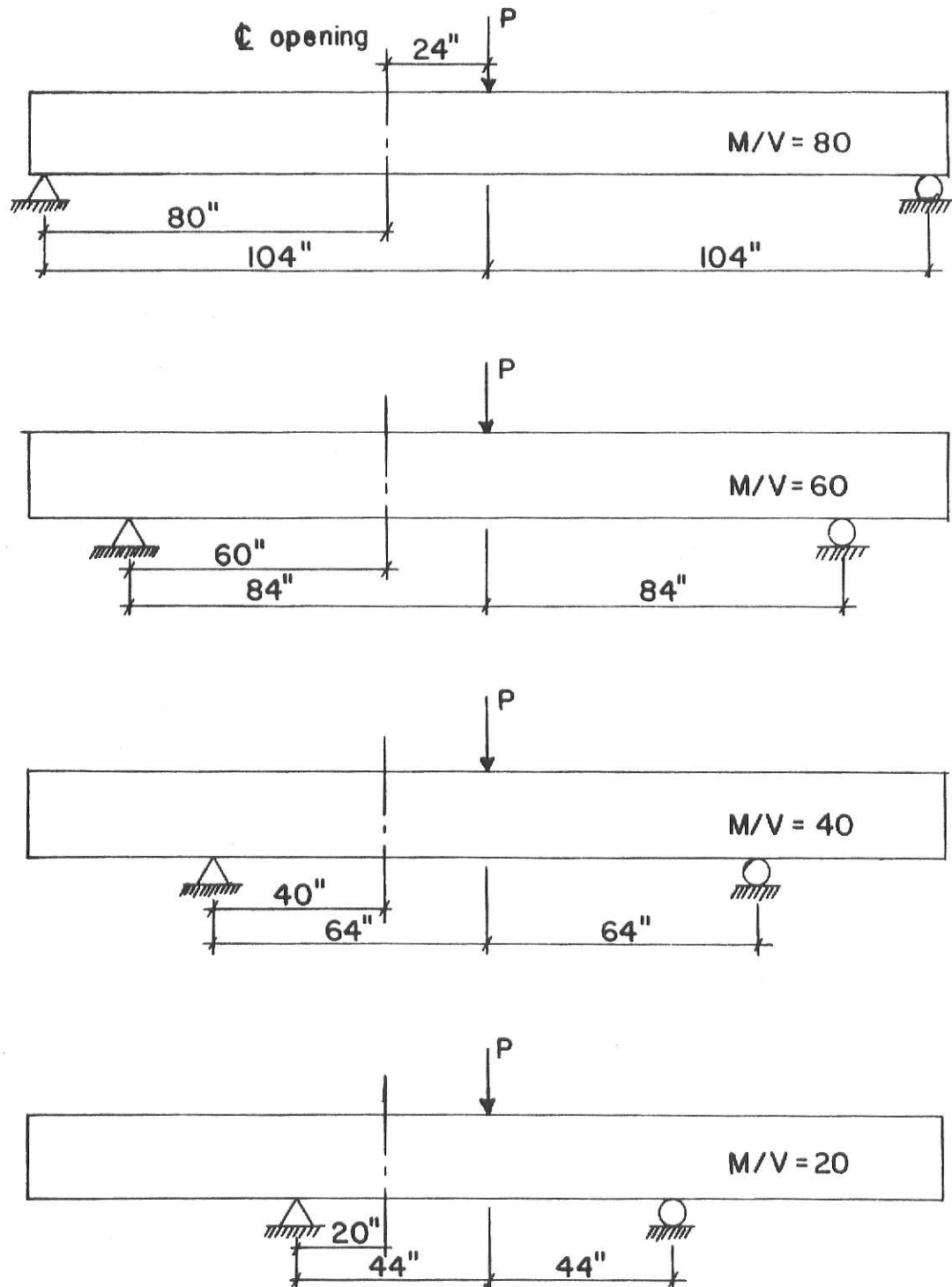


Fig. 4 - Test Setups

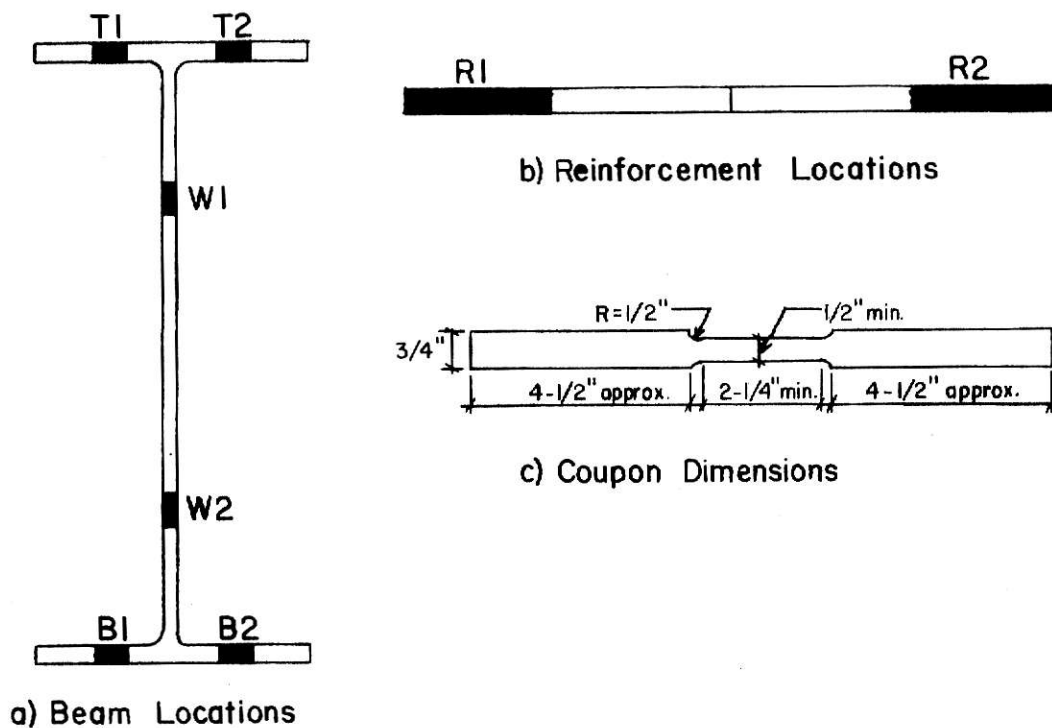


Fig. 6 — Tensile Specimen Details

Beam	Coupon	f_y (ksi)	f_u (ksi)	% Reduction In Area	% Elongation (In 2")
1	T1	43.12	---	56.5	27.9
	T2	43.98	80.07	57.9	32.5
	B1	43.94	80.11	57.5	31.3
	B2	43.89	80.59	58.3	31.3
	W1	43.65	76.61	54.8	31.5
	W2	41.46	75.68	60.7	35.3
2	T1	42.77	81.97	56.6	31.5
	T2	42.60	80.37	57.1	32.0
	R1	43.02	83.91	55.3	26.4
	B2	42.24	80.29	51.9	32.5
	W1	42.40	76.15	55.7	33.0
	W2	43.72	76.44	56.5	33.0
	R1	40.36	66.35	57.2	35.0
	R2	38.48	64.96	55.5	36.5

Table 1 - Tensile Test Results

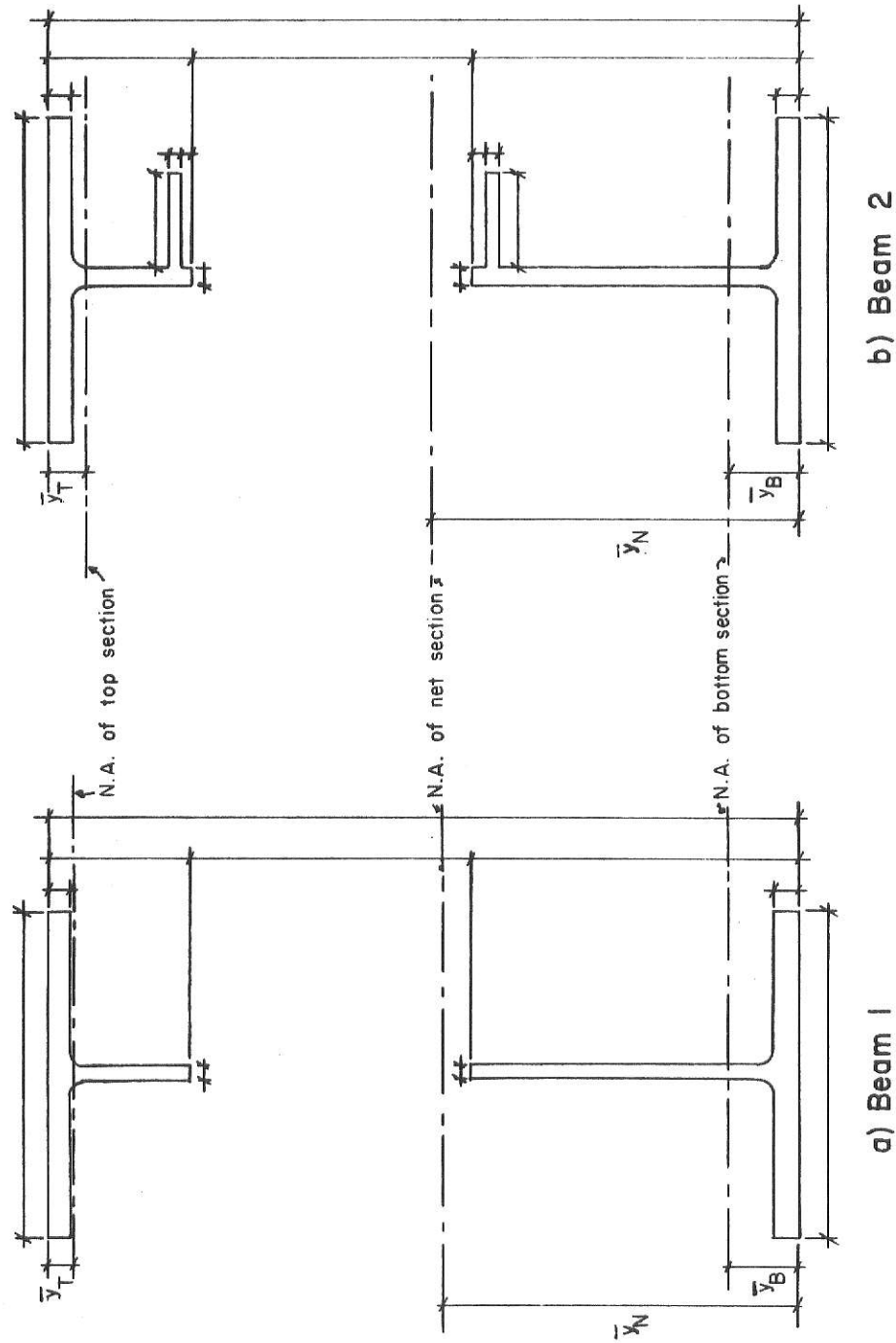


Fig. 7 — Cross-section Dimension Locations

	Nominal	Beam 1	Beam 2
Top Flange			
Width			
LME		6.970	7.010
HME		6.970	7.010
Average	7.039	6.970	7.010
Thickness			
LME		0.539	0.542
HME		0.538	0.541
Average	0.563	0.539	0.541
Web Thickness			
LME		0.371	0.379
HME		0.377	0.381
Average	0.346	0.374	0.380
Bottom Flange			
Width			
LME		7.020	6.960
HME		7.020	6.960
Average	7.039	7.020	6.960
Thickness			
LME		0.540	0.538
HME		0.538	0.536
Average	0.563	0.539	0.537
Depth			
LME		16.100	16.110
HME		16.100	16.110
Average	16.120	16.100	16.110
Tee Depth			
Top Tee	3.060	3.140	3.020
Bottom Tee	7.060	6.910	7.080
Opening Depth	6.000	6.050	6.010
Reinforcement			
Width	2.000		1.970
Thickness	0.250		0.241
Distance From			
Opening Edge			
Top Tee	0.250		0.230
Bottom Tee	0.250		0.310

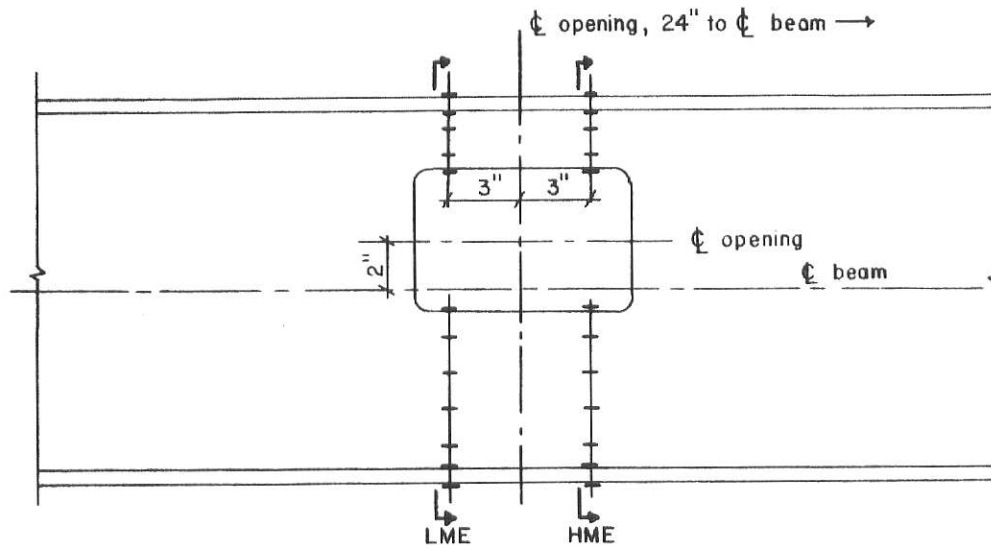
Table 2 - Cross-Sectional Dimensions
and Properties (At Opening)

	Nominal	Beam 1	Beam 2
Area			
Gross	13.30		
Net (In. ²)	11.04	10.91	
	12.04		11.91
Moment of Inertia			
Gross	584.00		
Net (In. ⁴)	560.87	546.03	
	577.44		561.87
Top Tee			
A	4.83	4.75	
	5.33		5.18
\bar{y}	0.56	0.59	
	0.76		0.77
I	2.21	2.55	
	4.27		4.22
Bottom Tee			
A	6.21	6.61	
	6.71		6.75
\bar{y}	1.56	1.61	
	1.94		2.03
I	25.89	25.58	
	38.05		38.63
\bar{y} Net Section	7.68	7.66	
	7.88		7.82

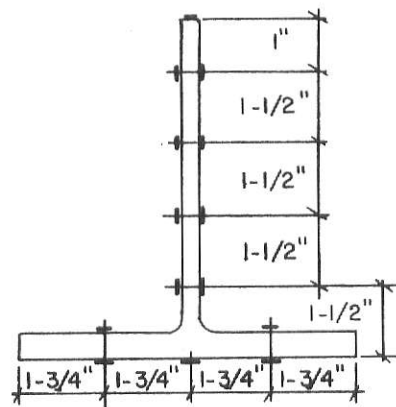
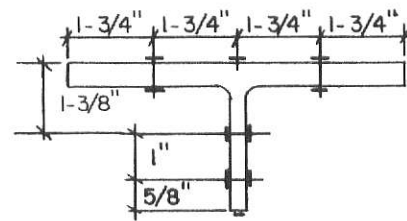
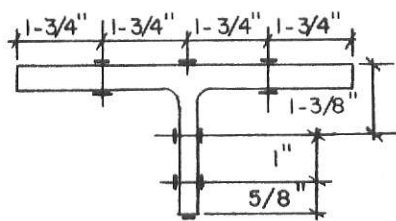
Table 2 (Con't) - Cross-Sectional Dimensions
and Properties (At Opening)

	Nominal	Beam 1	Beam 2
Top Flange			
Width			
Left		6.980	7.037
Right		6.970	7.040
Average	7.039	6.975	7.039
Thickness			
Left		0.535	0.543
Right		0.543	0.540
Average	0.543	0.539	0.542
Web Thickness			
Left		0.383	0.381
Right		0.384	0.382
Average	0.346	0.384	0.382
Bottom Flange			
Width			
Left		7.020	6.970
Right		7.030	7.014
Average	7.039	7.025	6.992
Thickness			
Left		0.537	0.535
Right		0.545	0.539
Average	0.546	0.541	0.537
Depth			
Left		16.080	16.106
Right		16.120	16.100
Average	16.120	16.100	16.103

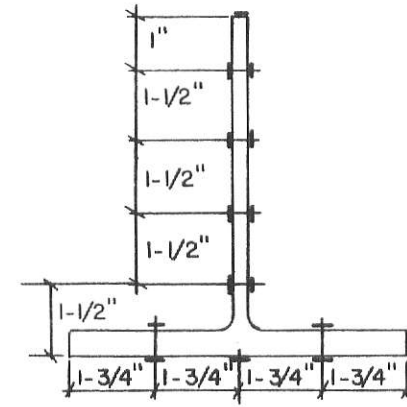
Table 3 - Cross-Sectional Dimensions
(At Ends)



a) Opening Elevation

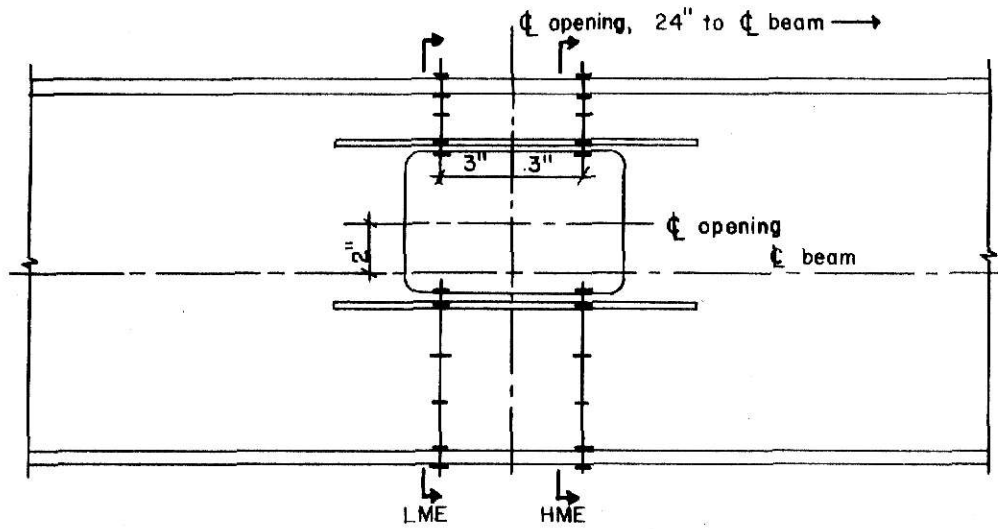


b) Low Moment Edge



c) High Moment Edge

Fig. 8— Strain Gage Locations — Beam I



a) Opening Elevation

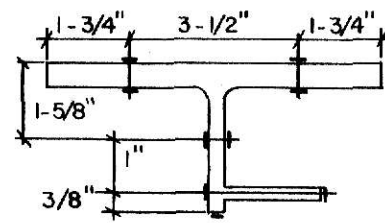
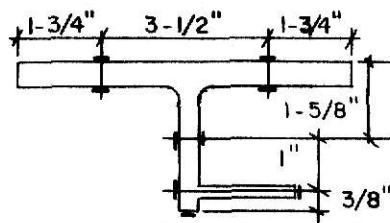


Diagram of a T-section for the Low Moment Edge condition. The section has a top flange with a thickness of $3/8"$ and a width of $2"$. The web has a height of $2"$ and a thickness of $2-5/8"$. The bottom flange has a thickness of $1-3/4"$ and a width of $3-1/2"$. The total width of the bottom flange is $1-3/4" + 3-1/2" + 1-3/4" = 6-1/2"$.

c) High Moment Edge

Fig. 9 — Strain Gage Locations — Beam 2

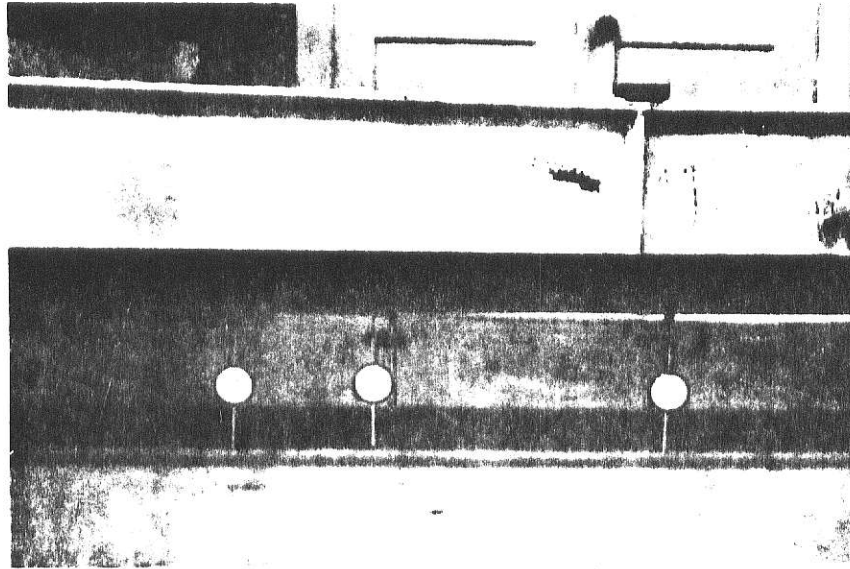


Fig. 10a -- Elevation of Dial Gage Support System

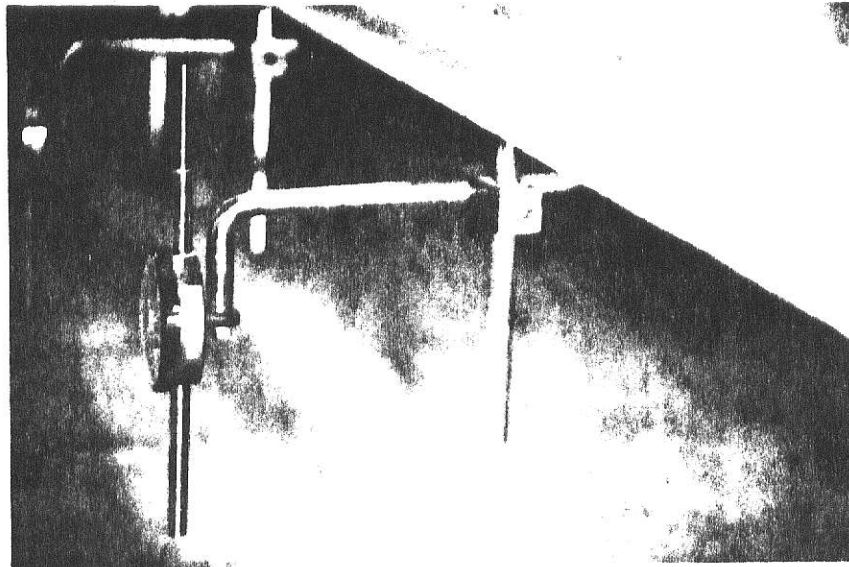


Fig. 10b -- Individual Dial Gage Support

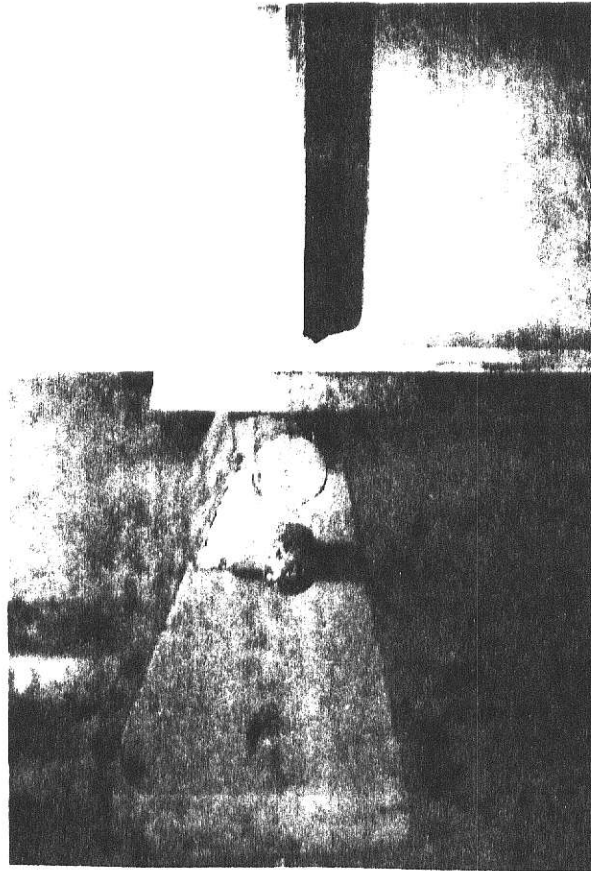


Fig. 11 -- Support Pedestal

	Beam 1					Beam 2				
	Midspan δ (in.)	HME δ (in.)	LME δ (in.)	Relative δ Across Opening	Midspan δ (in.)	HME δ (in.)	LME δ (in.)	Relative δ Across Opening		
M/V										
80	0.238	0.227	0.210	0.017	0.222	0.209	0.196	0.013		
60	0.131	0.121	0.109	0.012	0.119	0.110	0.098	0.012		
40	0.064	0.056	0.046	0.010	0.056	0.049	0.040	0.009		
20	0.027	0.020	0.013	0.007	0.023	0.018	0.011	0.007		

Table 4 - Deflection Readings For 20^k Load

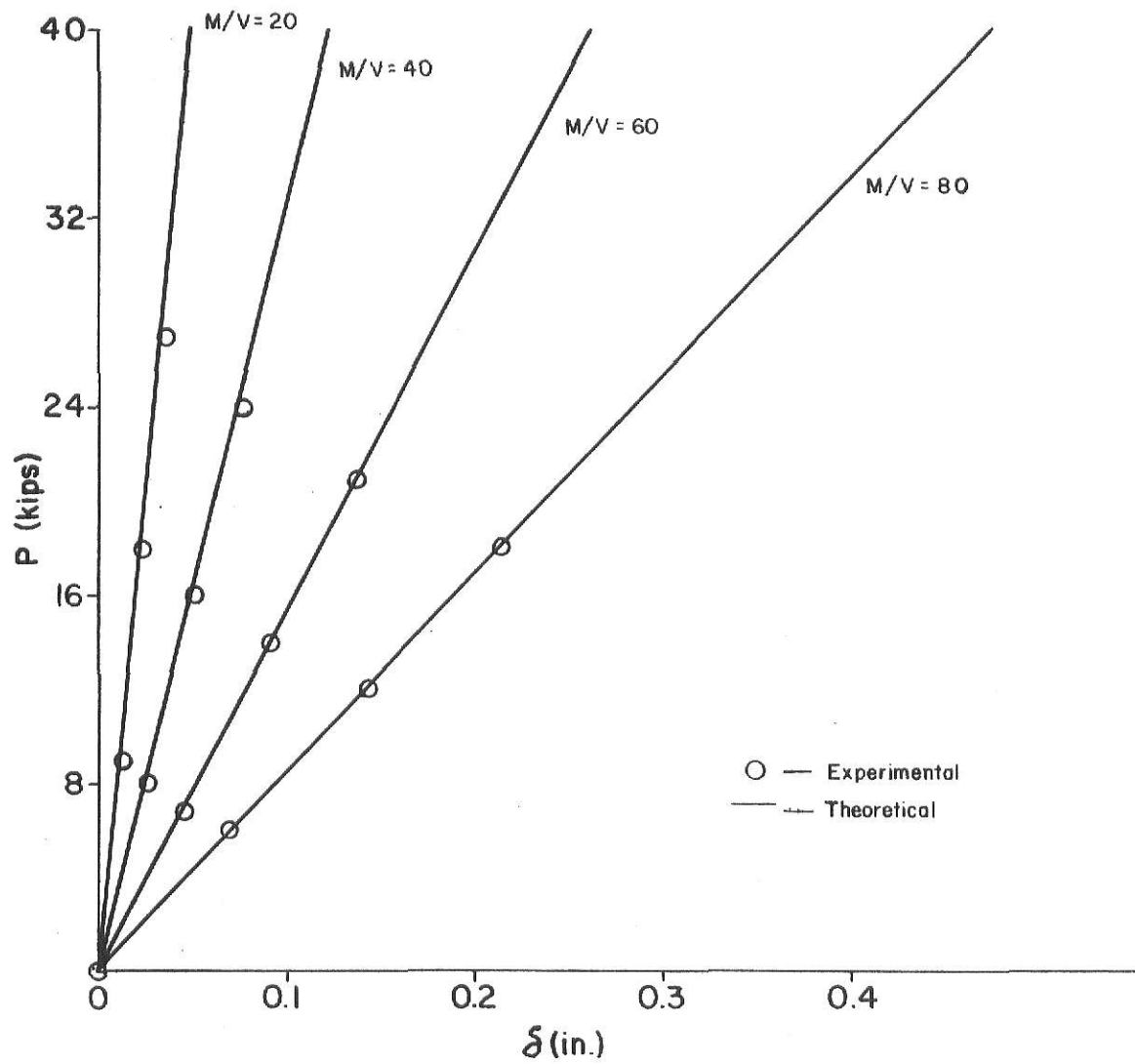


Fig. 12 — Load vs. Midspan Deflection — Elastic Load Tests — Beam 1

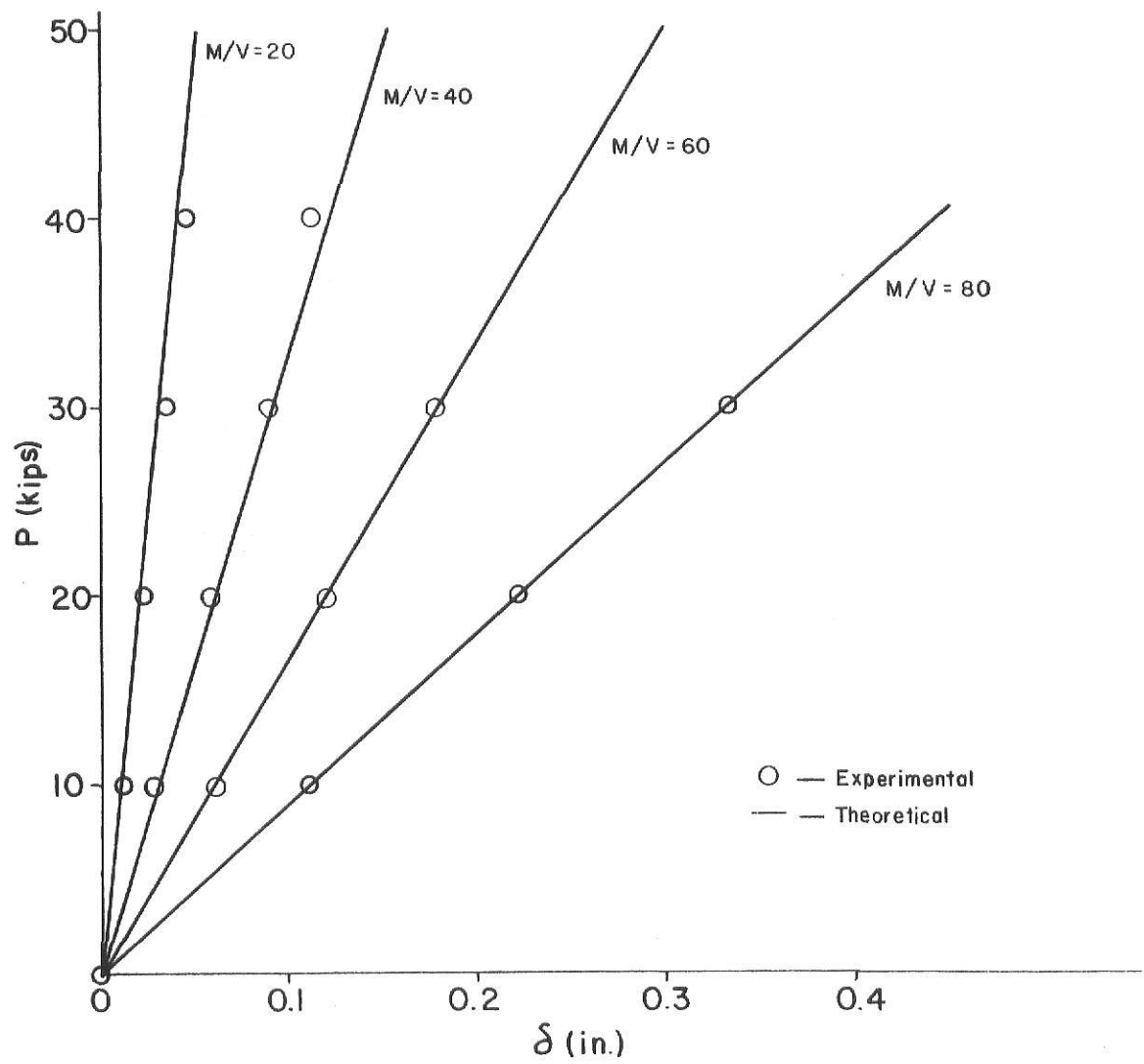


Fig. 13 — Load vs. Midspan Deflection — Elastic Load Tests — Beam 2

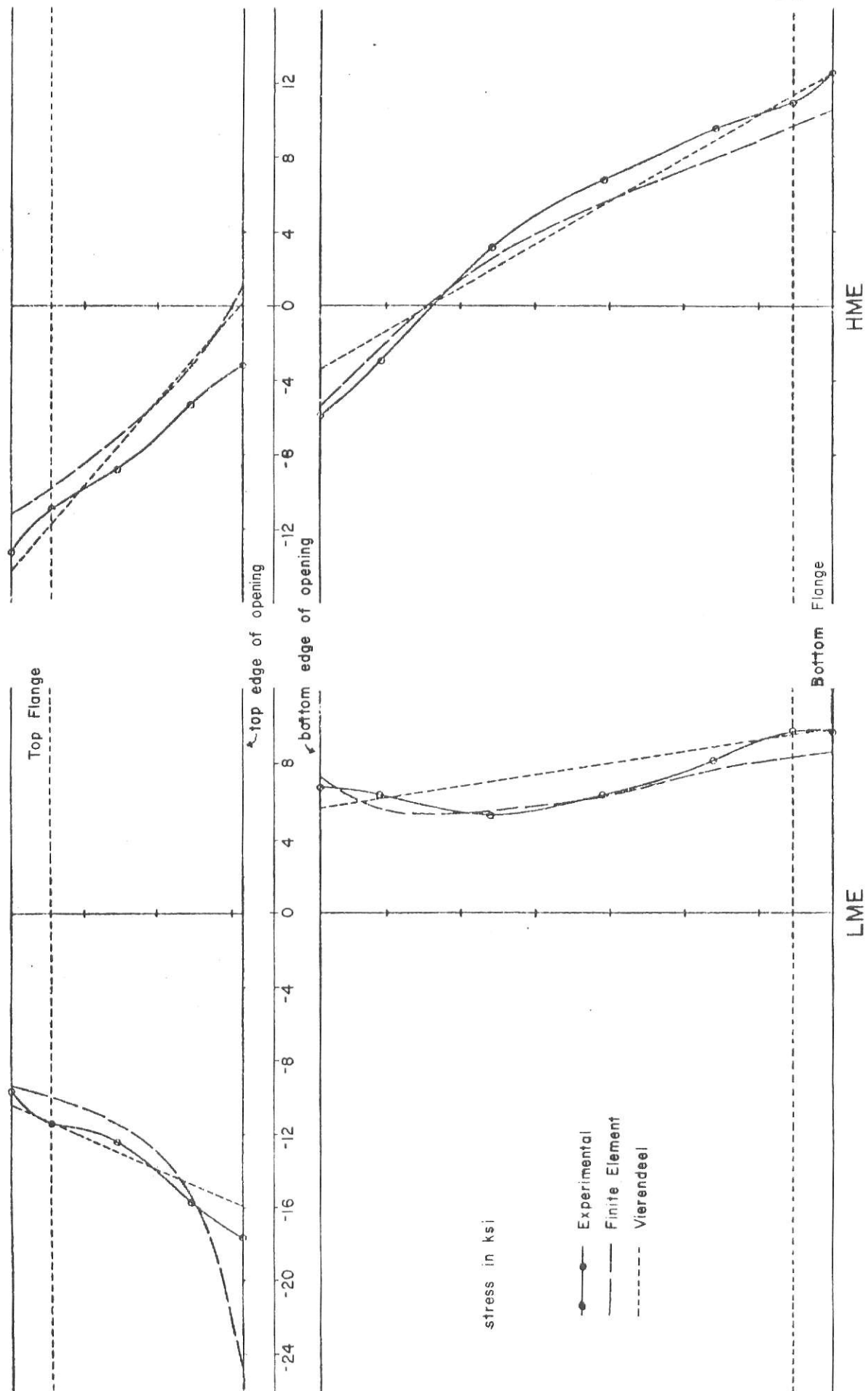


Fig. 14 — Stress Distribution Curves — Beam 1 — $M/V = 80$

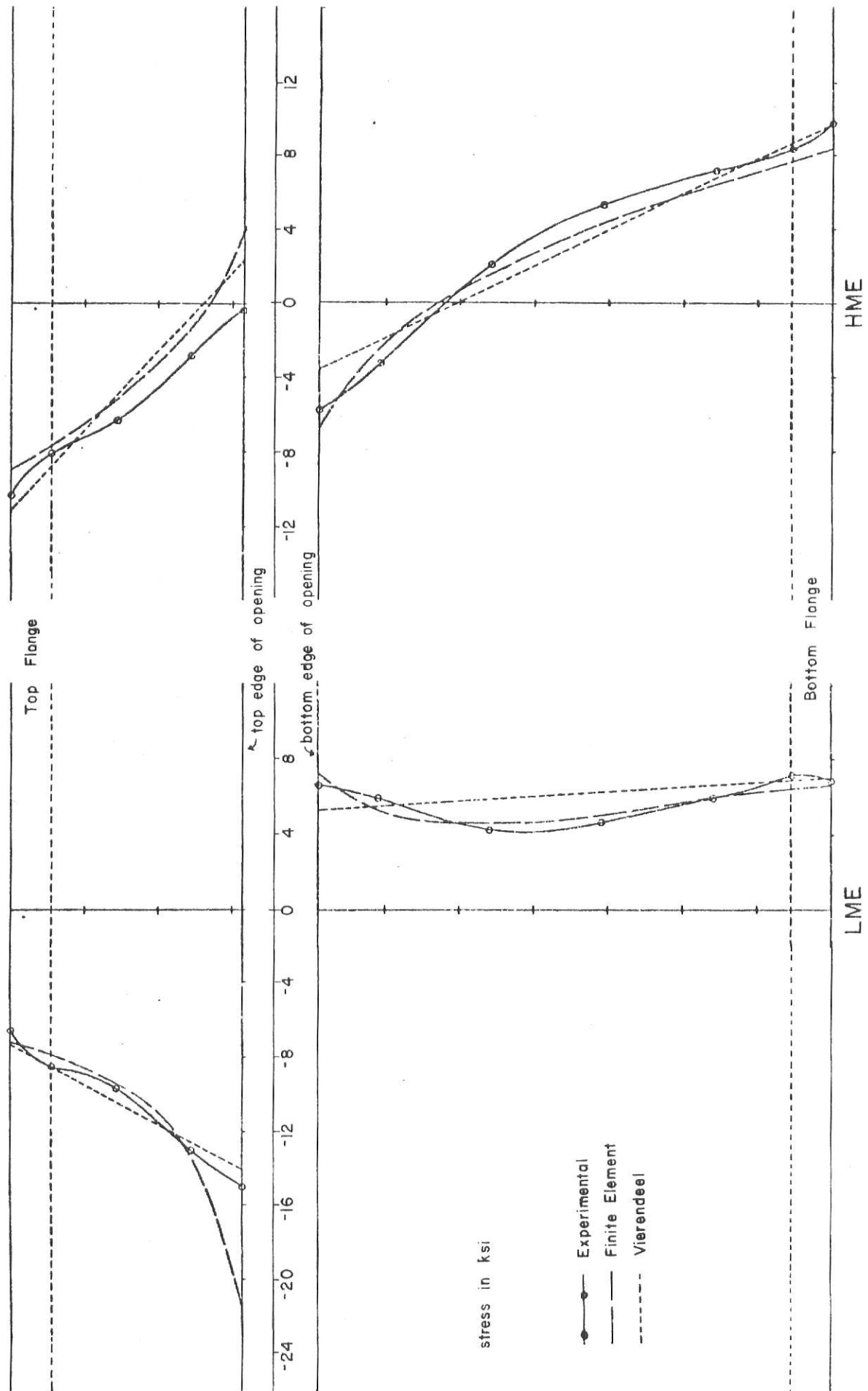
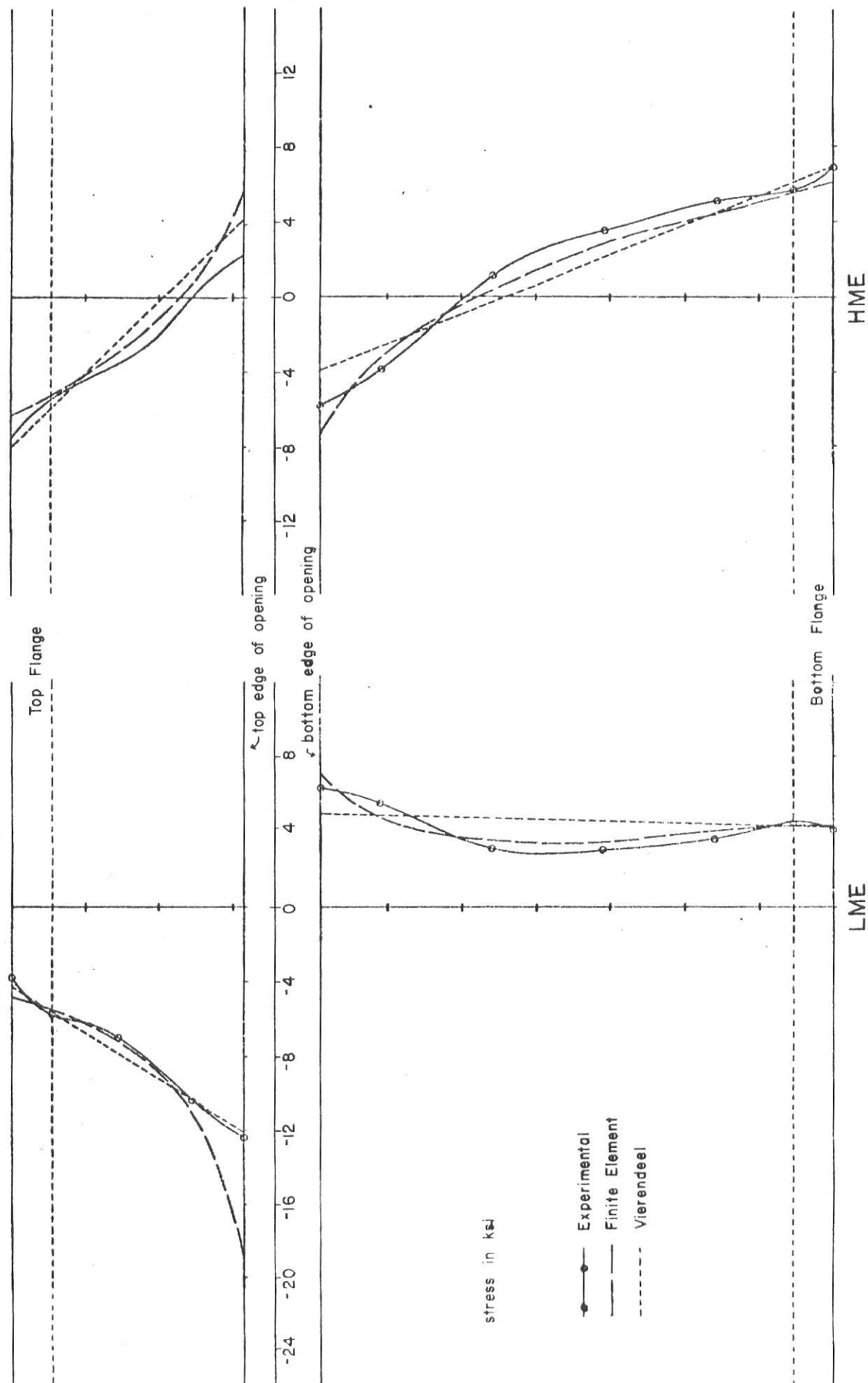


Fig. 15— Stress Distribution Curves — Beam 1 — $M/V = 60$

Fig. 16 — Stress Distribution Curves — Beam 1 — $M/V=40$

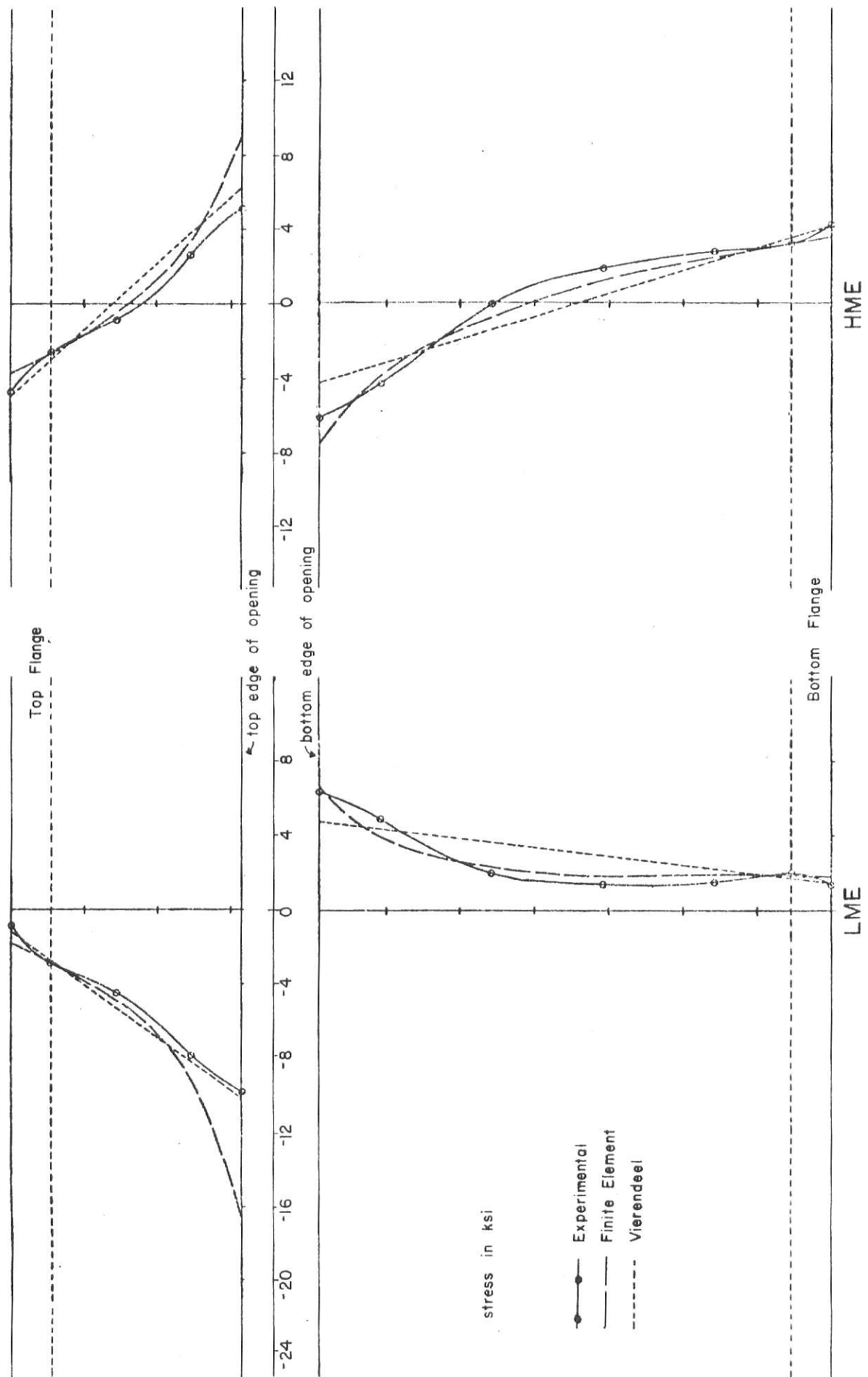


Fig. 17 — Stress Distribution Curves — Beam 1 — $M/V=20$

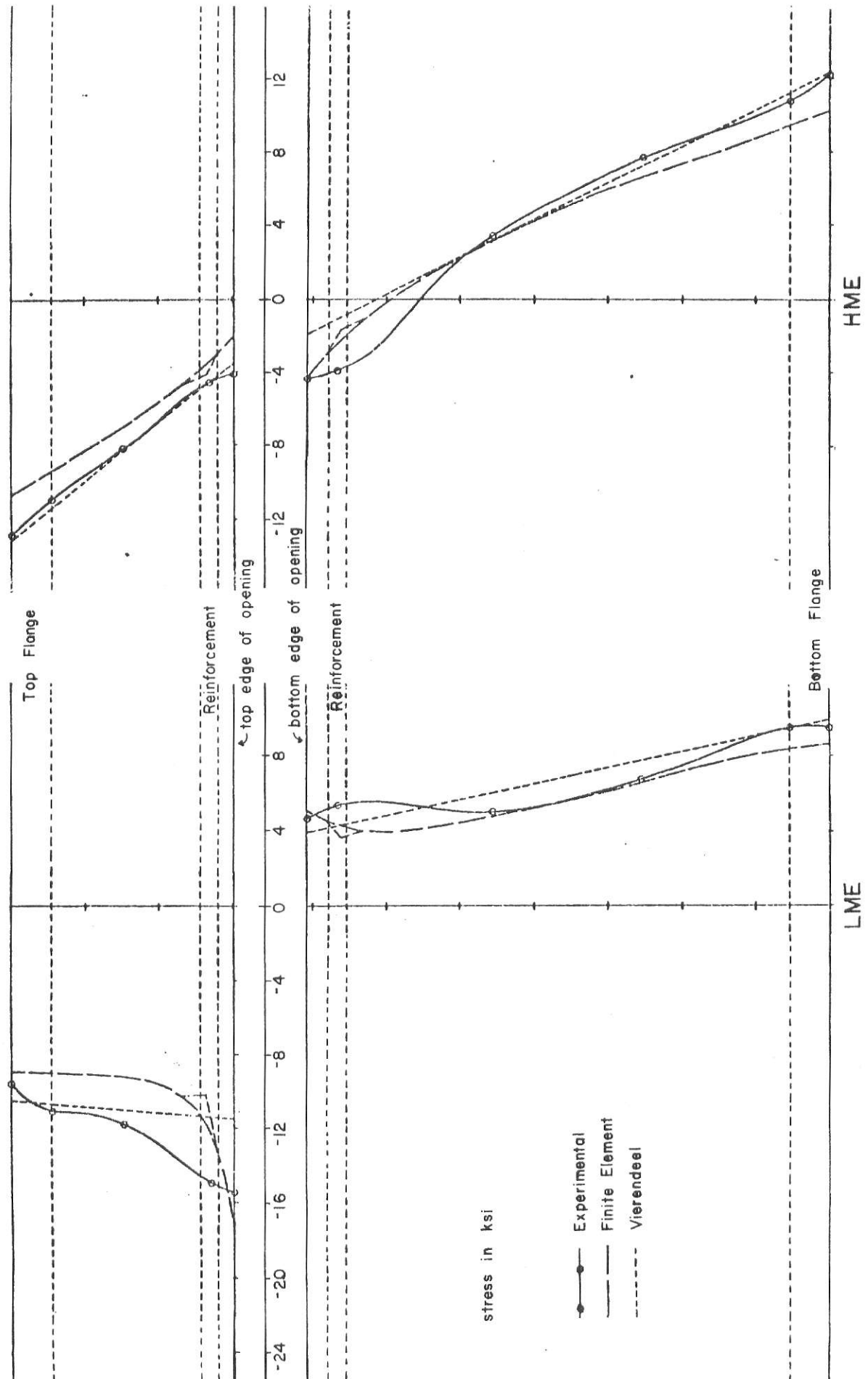
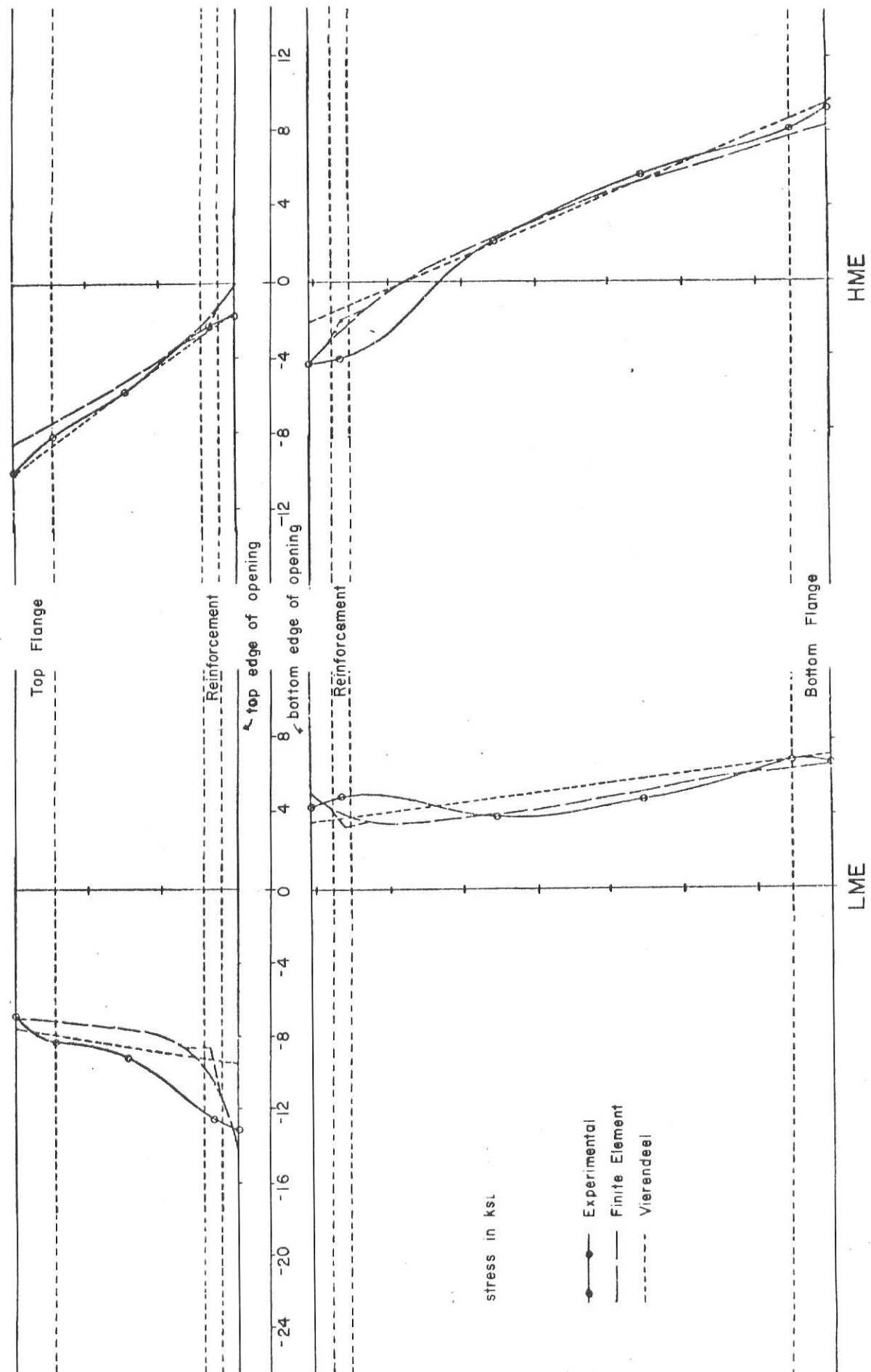
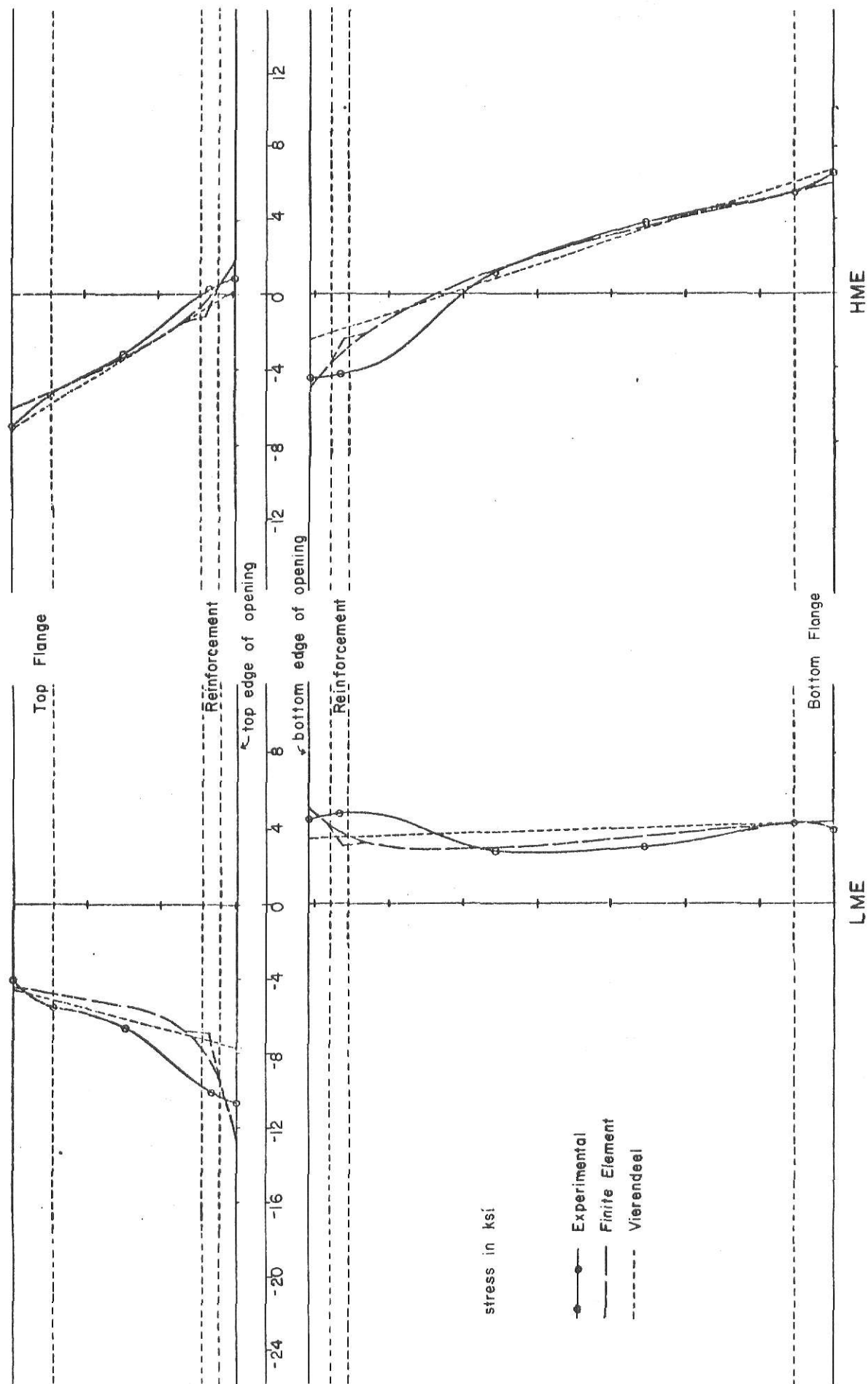
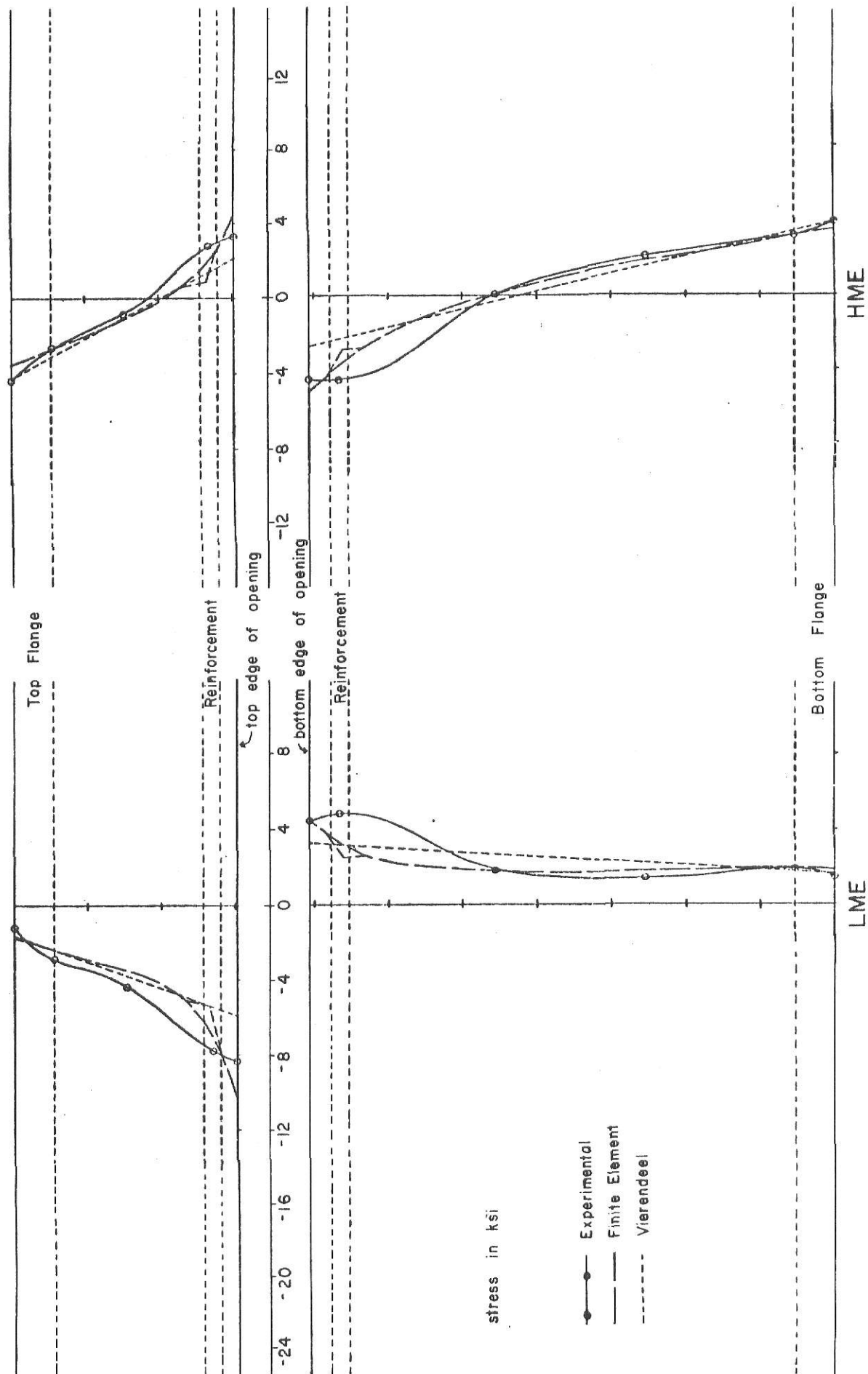


Fig. 18 — Stress Distribution Curves — Beam 2 — $M/V = 80$

Fig. 19 — Stress Distribution Curves — Beam 2 — $M/V = 60$

Fig. 20 — Stress Distribution Curves — Beam 2 — $M/V = 40$

Fig. 21 — Stress Distribution Curves — Beam 2 — $M/V = 20$

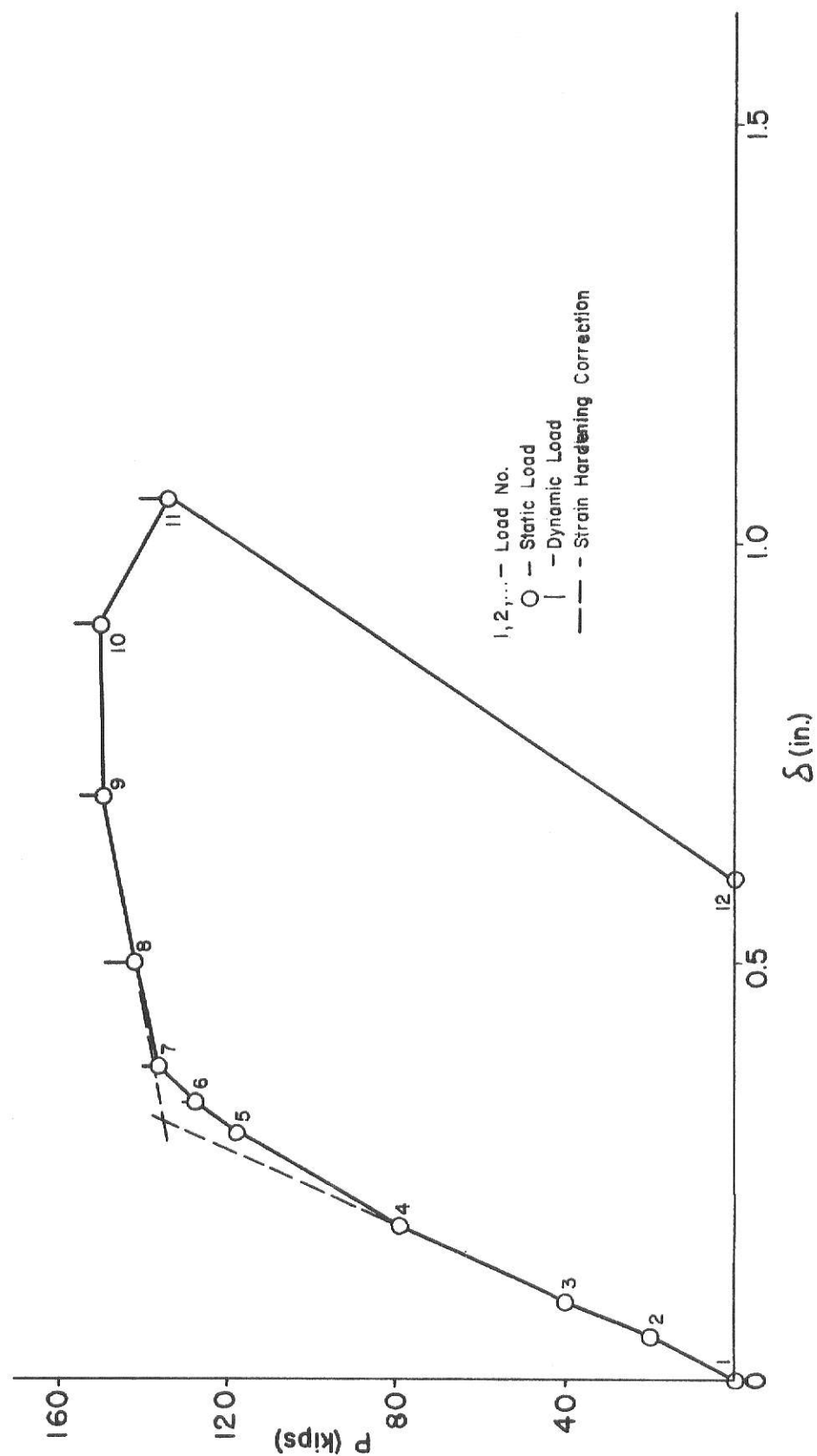


Fig. 22 — Load vs. Midspan Deflection — Ultimate Load Test — Beam I

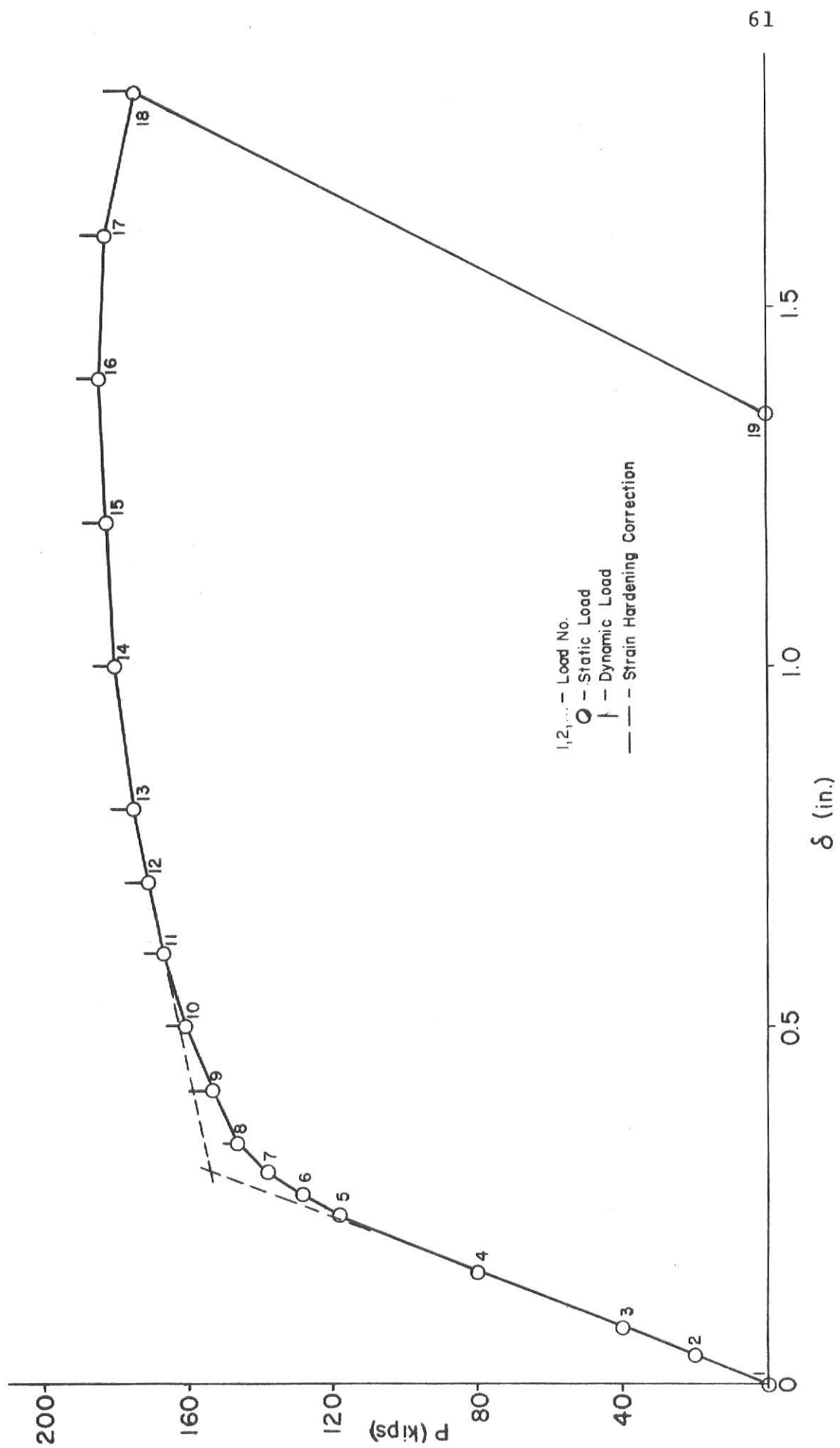


Fig. 23 - Load vs. Midspan Deflection - Ultimate Load Test - Beam 2

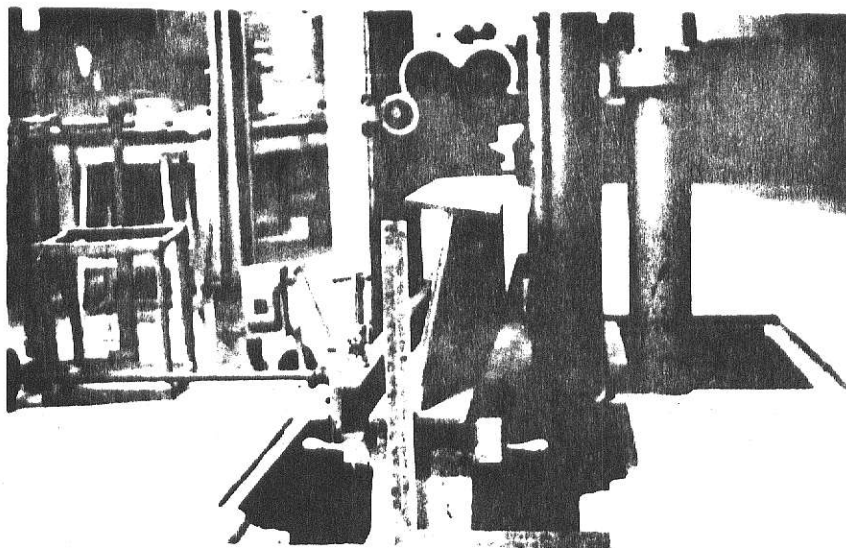


Fig. 24a -- Lateral Displacement of Compression Flange of Beam 1 at Failure

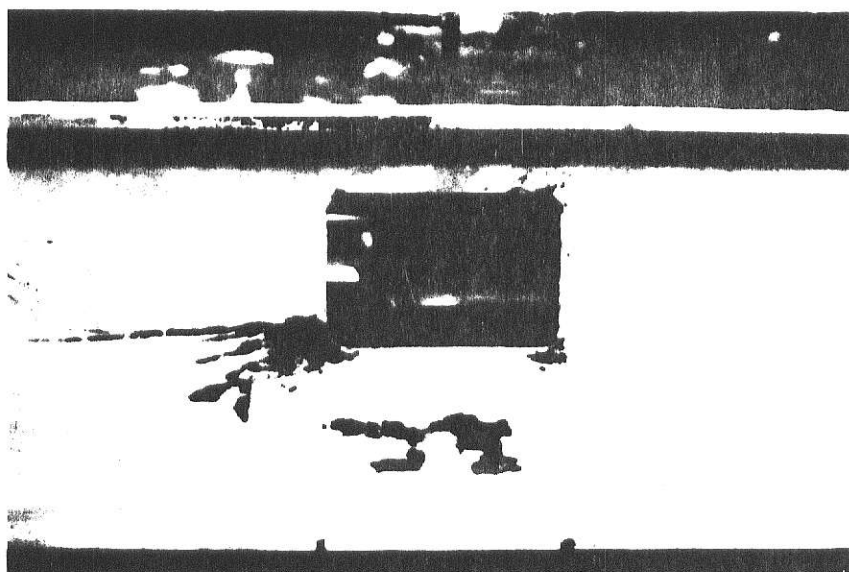


Fig. 24b -- Elevation of Opening in Beam 1 After Ultimate Load Test

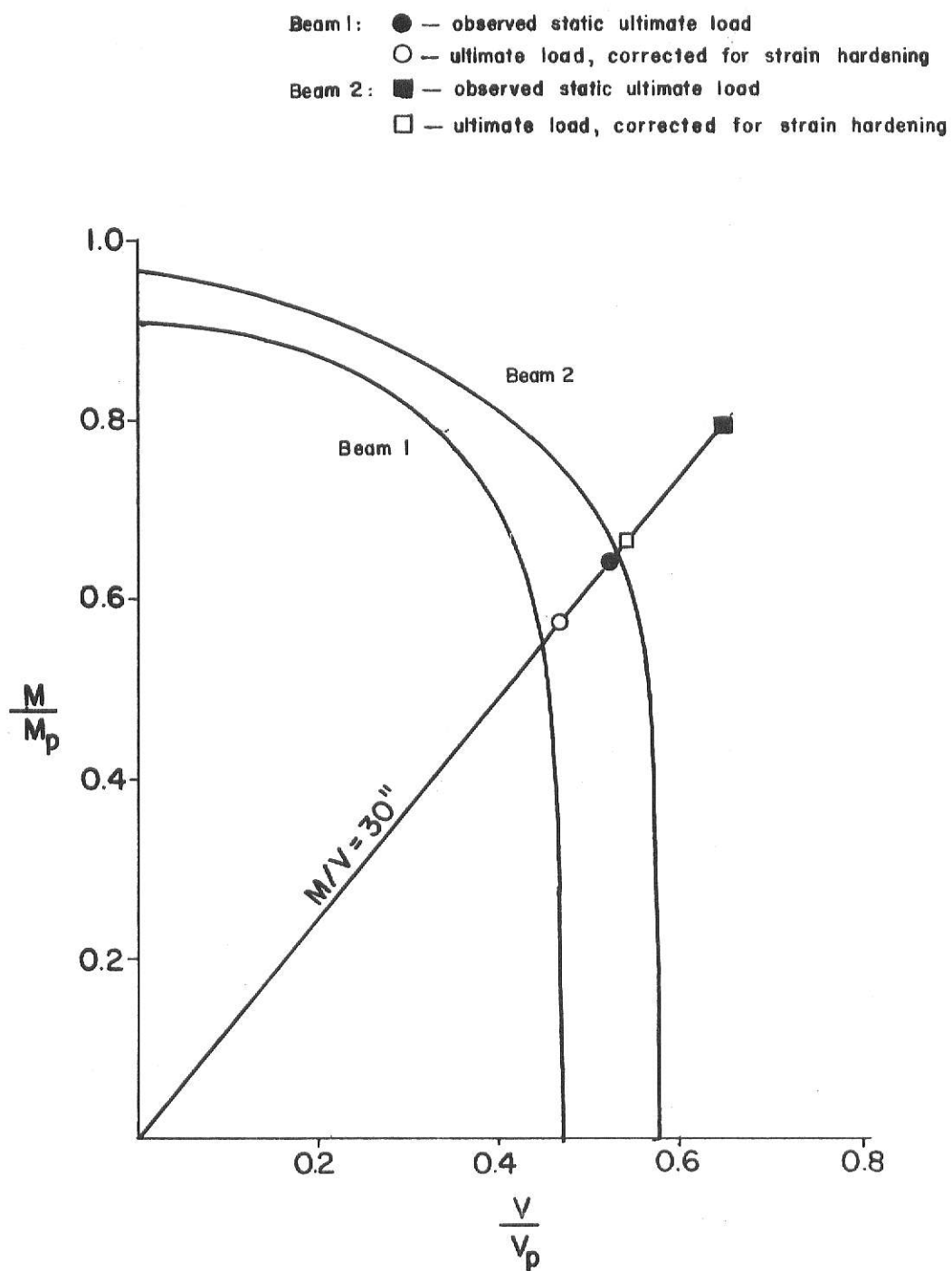


Fig. 25 — Interaction Curves

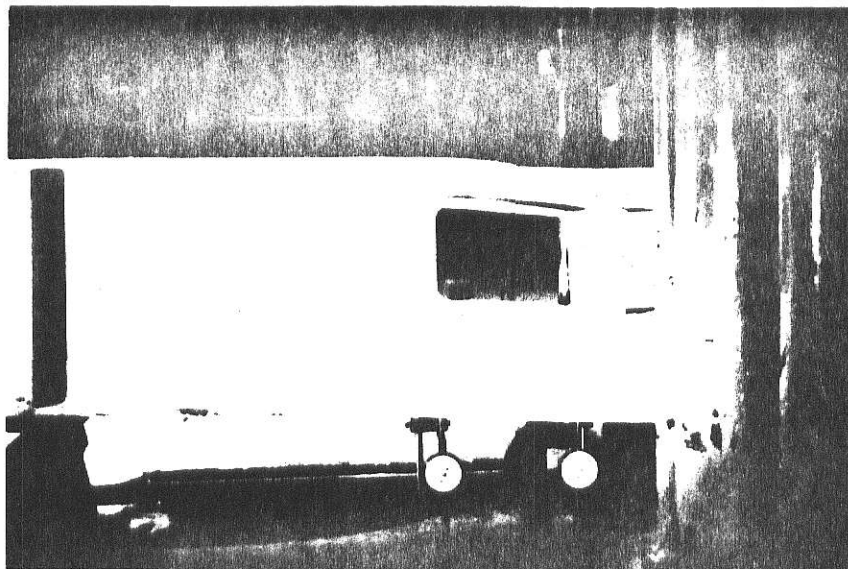


Fig. 26a -- Elevation of Opening in Beam 2
After Ultimate Load Test

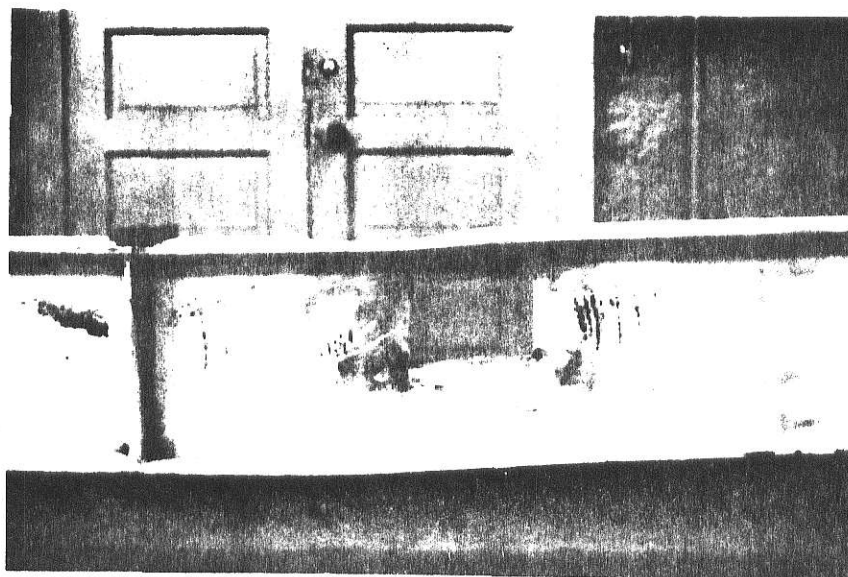


Fig. 26b -- Elevation of Opening in Beam 2
After Ultimate Load Test

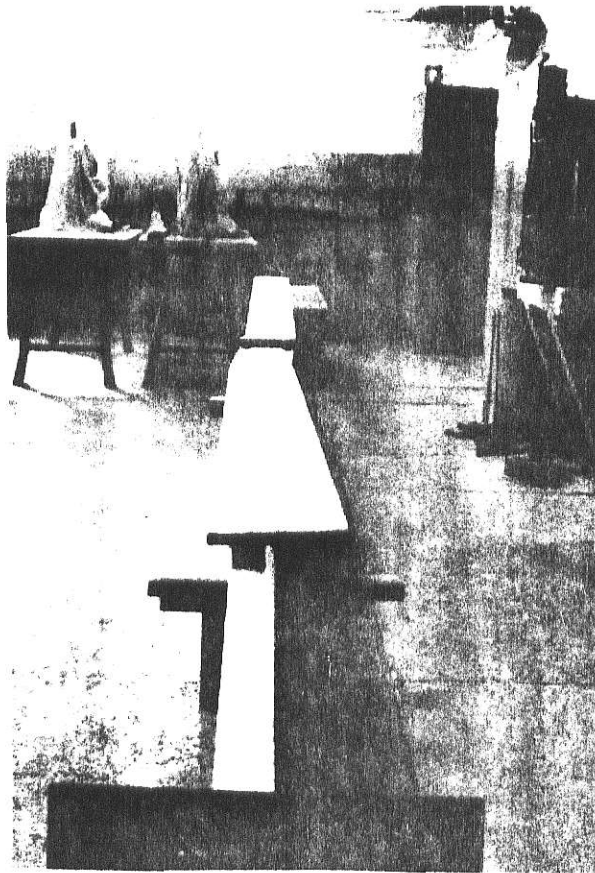


Fig. 26c -- Compression Flange of Beam 2
After Ultimate Load Test

EXPERIMENTAL TESTS OF BEAMS
WITH ECCENTRIC WEB OPENINGS

by

Jerry Lynn McNew

B. Arch., Kansas State University, 1973

AN ABSTRACT OF A MASTER'S THESIS

submitted in partial fulfillment of the

requirements for the degree

MASTER OF SCIENCE

Department of Civil Engineering

Kansas State University

Manhattan, Kansas

1974

ABSTRACT

At times it becomes necessary to cut openings in the webs of structural steel members to allow for the passage of ductwork, pipes, and wires. Because of the physical requirements of these systems, the centerlines of the openings don't always coincide with the centerlines of the beams.

In the present investigation, tests were conducted on two W16 x 45 A36 steel beams with 6 inch deep by 9 inch long openings positioned 2 inches above the centerline of the beam. The opening was unreinforced in Beam 1 and reinforced in Beam 2. Elastic tests were conducted at moment-shear ratios of 80, 60, 40, and 20. Ultimate load tests were conducted at a moment-shear ratio of 30.

Generally it was found that the elastic stresses could be fairly accurately predicted using the Finite Element or Vierendeel Methods of Analysis. It was also found that the moment-shear ratio had very little effect on the ratio of the distribution of the shearing force to the beam sections above and below the opening.

For the ultimate load tests, it was found that the failure load of the beam could be quite accurately predicted using ultimate strength theory. Also, the presence of reinforcement significantly increased the load carrying capacity of the beam.